J Neurophysiol 107: 2833–2852, 2012.
First published February 29, 2012; doi:10.1152/jn.00709.2011.

Subthreshold somatic voltage in neocortical pyramidal cells can control whether spikes propagate from the axonal plexus to axon terminals: a model study

Erin Munro[1,2] and Nancy Kopell[2]

[1]*Laboratory for Neural Computation and Adaptation, RIKEN Brain Science Institute, Saitama, Japan; and* [2]*Mathematics Department, Boston University, Boston, Massachusetts*

Submitted 29 July 2011; accepted in final form 22 February 2012

Munro E, Kopell N. Subthreshold somatic voltage in neocortical pyramidal cells can control whether spikes propagate from the axonal plexus to axon terminals: a model study. *J Neurophysiol* 107: 2833–2852, 2012. First published February 29, 2012; doi:10.1152/jn.00709.2011.—There is suggestive evidence that pyramidal cell axons in neocortex may be coupled by gap junctions into an "axonal plexus" capable of generating very fast oscillations (VFOs) with frequencies exceeding 80 Hz. It is not obvious, however, how a pyramidal cell in such a network could control its output when action potentials are free to propagate from the axons of other pyramidal cells into its own axon. We address this problem by means of simulations based on three-dimensional reconstructions of pyramidal cells from rat somatosensory cortex. We show that somatic depolarization enables propagation via gap junctions into the initial segment and main axon, while somatic hyperpolarization disables it. We show further that somatic voltage cannot effectively control action potential propagation through gap junctions on minor collaterals; action potentials may therefore propagate freely from such collaterals regardless of somatic voltage. In previous work, VFOs are all but abolished during the hyperpolarization phase of slow oscillations induced by anesthesia in vivo. This finding constrains the density of gap junctions on collaterals in our model and suggests that axonal sprouting due to cortical lesions may result in abnormally high gap junction density on collaterals, leading in turn to excessive VFO activity and hence to epilepsy via kindling.

gap junction; pyramidal cell; neocortex; very fast oscillation; epilepsy

AN AXONAL PLEXUS IS A NETWORK of axons connected by gap junctions. Such networks were proposed by Roger Traub and colleagues as a mechanism for very fast oscillations (VFOs; >80 Hz) in the neocortex and hippocampus (Traub et al. 1999, 2001, 2003a,b, 2005a, 2010). While chemical synapses operate on a time scale that is too slow to support VFOs, gap junctions can transmit action potentials (APs) within a fraction of a millisecond.

Putative gap junctions connecting pyramidal cell axons have been observed in several areas of the cortex. Wang et al. (2010) reported gap junctions close to pyramidal cell somata in 5% of paired recordings taken from layer 5 of rat neocortex, where somata are adjacent. Hamzei-Sichani et al. (2007) demonstrated the existence of gap junctions on hippocampal mossy fibers by immunogold labeling. Somatic spikelets of 5–15 mV indicate the presence of axonal gap junctions (Draguhn et al. 1998; Mercer et al. 2006) and are seen in 30% of cells during the depolarization phase of slow-wave sleep oscillations (Steriade et al. 1993). Dye-coupling studies have also demonstrated axonal gap junctions in the hippocampus and neocortex (Gutnick et al. 1985; Gutnick and Prince 1981; Schmitz et al. 2001).

Despite such evidence, the prevalence and significance of gap junctions connecting pyramidal cell axons remain controversial. While gap junctions connecting interneurons are plentiful, gap junctions among pyramidal cell axons have been difficult to find. Moreover, the channel proteins of putative axo-axonal gap junctions have not been established, so many of the techniques used to identify and study interneuron gap junctions are not available.

The functional significance of axo-axonal gap junctions has also been called into question. If there is a large network of pyramidal cell axons that are connected to each other by gap junctions, then how could individual pyramidal cells control whether APs from other axons in the network propagate into their main axons and down to their axon terminals? In this study, we address this issue of control.

Activity associated with gap junctions in the normal neocortex appears to be controlled by the somatic voltage. Wang et al. (2009b) showed individual pyramidal cells firing with millisecond synchrony in low calcium media only when cells were in a depolarized state. VFOs, which are presumably generated by an axonal plexus, are prevalent during depolarized states. Grenier et al. (2001) showed VFOs during the up-state of slow oscillations. The amplitude of VFOs drops significantly during the down-state, and VFOs are abolished by the gap junction blocker halothane. VFOs also occur in active areas during neocortical processing (Brosch et al. 2002; Brovelli et al. 2005; Canolty et al. 2007; Cheyne et al. 2008; Edwards et al. 2005, 2009; Gaona et al. 2011; Jacobs and Kahana 2009; Jones and Barth 1999; Jones et al. 2000; Pei et al. 2011; Roland et al. 2010; Wang et al. 2009a). [See Crone et al. (2006) for a review.]

In previous work, Munro and Börgers (2010) showed that the somatic voltage can control AP propagation across axonal-gap junctions in a simple axonal model in which all gap junctions are located on the same spot in the axon. However, neocortical pyramidal cell axons have complex geometries, and gap junctions are not likely to be in the same location. Thus it remains to establish whether control is still possible in more realistic networks.

In this work, we use three-dimensional (3D) reconstructions of pyramidal cells to model the affect of somatic voltage on AP propagation across gap junctions in different locations in the axon: the initial segment (IS), the main axon, and collaterals.

Address for reprint requests and other correspondence: E. Munro, RIKEN Brain Science Institute, 2-1Hirosawa, Wako, Saitama 351-0198, Japan (e-mail: erin.munro@brain.riken.jp).

We use simulations to show that the somatic voltage can control propagation across gap junctions in the IS and main axon but cannot control AP propagation from axon collaterals. Since the somatic voltage may not control AP propagation across all gap junctions, there may be cells "hardwired" together by gap junctions, in the sense that whenever one cell fires, the other fires as well, regardless of somatic voltage. However, we will argue that data from field potential recordings and analysis of a gap junction network indicate that the number of cells hardwired together in this sense is limited in the normal neocortex.

Our results suggest that individual pyramidal cells can adjust their subthreshold somatic voltage to control whether APs propagate from the axonal plexus into their main axon. A depolarized somatic voltage allows APs to propagate into the main axon, while a hyperpolarized somatic voltage prevents APs from propagating into the main axon, as illustrated in Fig. 1. Therefore, pyramidal cell somata do not have to fire to send spikes to axon terminals, but can signal post (chemical) synaptic cells by adjusting their somatic voltage. (In this study, we will use the terms "presynaptic" and "postsynaptic" to refer to chemical synapses.) Moreover, abnormally high numbers of gap junctions on collaterals, possibly resulting from cortical lesions or axonal sprouting, may lead to a large number of pyramidal cells that are hardwired together. This may lead to VFOs that cannot be stopped by somatic hyperpolarization. Such persistent VFOs can lead to epilepsy by kindling postsynaptic neighbors.

Glossary

Definitions

Hardwired together	Two cells are hard wired together if APs propagate from one axon to another regardless of somatic voltage
Window of control	Values of g_{Na} where $g_{Na,-60} \leq g_{Na} \leq g_{Na,-80}$

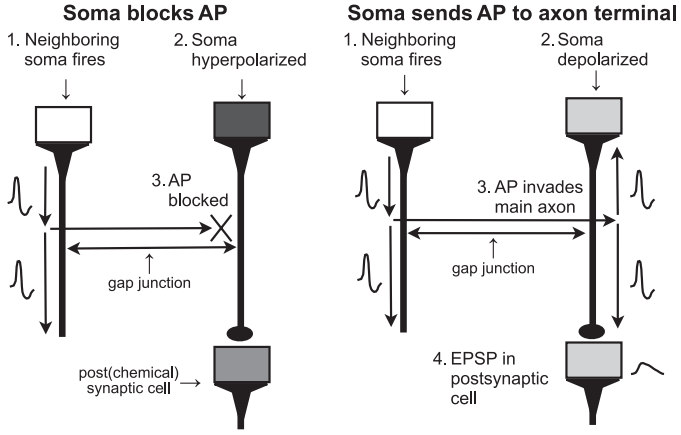

Fig. 1. Illustration of how the subthreshold somatic voltage of a pyramidal cell may control action potential (AP) propagation across gap junctions into its main axon. Our simulations show that when the soma is hyperpolarized, APs are blocked at the gap junction. When the soma is depolarized, APs are allowed to invade the main axon and propagate down to axon terminals. In this manner, a pyramidal cell can send spikes to its axon terminals and signal post(chemical)synaptic cells by adjusting their subthreshold somatic voltage. EPSP, excitatory postsynaptic potential.

Acronyms

AP	Action potential
IS	Initial segment
MA	Main axon
VFO	Very fast oscillation, oscillation >80 Hz

Cell Morphology

d_{IS}	IS diameter
d_{MA}	Main axon diameter
d_S	Soma diameter
ℓ_c	Electrotonic length of the sharp taper from the soma to the IS
l_c	Length of sharp taper from soma to IS in μm
λ	1 electrotonic length
s_{ratio}	d_S/d_{IS}

Physiology

C	Capacitance
g_{gj}	Gap junction conductance
g_K	Potassium conductance
g_L	Leak conductance
g_{Na}	Sodium conductance
g_{Na,V_s}	Threshold sodium conductance for AP propagation into the receiving cell, whose somatic leak reversal potential is V_s
t	Time
V	Voltage
V_K	Reversal potential for potassium current
V_L	Reversal potential for leak current
V_{Na}	Reversal potential for sodium current
V_s	Reversal potential of leak current in the soma

Network Parameters

L	Mean weight of all cells in network
M	Number of cells within r_c of a single cell in network
m_{cy}	Average number of cycles
n	Mean size of largest cluster in network
n_{cc}	Number of cells per column
n_{cy}	Number of cells in largest cluster when $m_{cy} = 1$
N_O	Maximum number of cells hardwired together that will not produce VFOs
p	Probability of two axons connecting by a collateral gap junction per μm^2 in network model
p_4	Value of p that yields an average of ~4 connections per cell
p_{intra}	Probability of two axons connecting by an IS/MA gap junction within a column in network model
r_c	Maximum distance between connected cells in network model

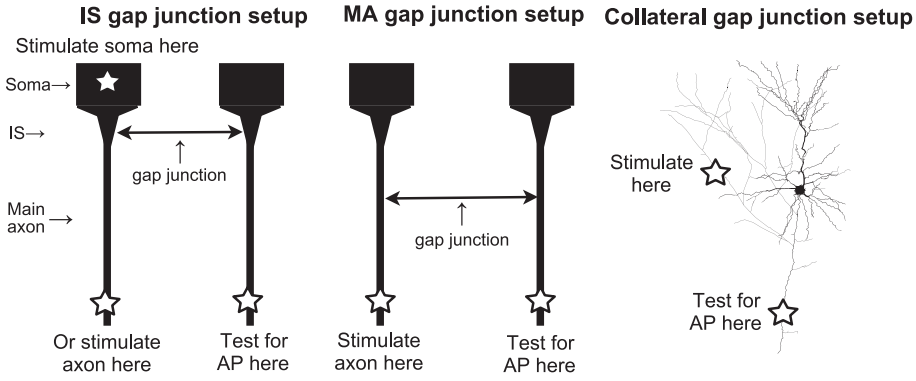

Fig. 2. Simulation setups to test for AP propagation across a gap junction. To test AP propagation across a gap junction in the initial segment (IS) and main axon (MA), we used two simplified axon models from the same layer. When the gap junction was in the IS, we stimulated the soma or the IS. When the gap junction was in the main axon, we stimulated only the distal axon of 1 cell. In both cases, we tested for AP propagation in the distal axon of the neighboring cell. To test AP propagation from a gap junction in an axon collateral, we used the exact geometry of the three-dimensional cell reconstructions. We stimulated the collateral so that it fired, and then tested for AP propagation in the main axon.

Field Potential

m_{max}	Number of cells that generated the maximum VFO amplitude observed
N_{VFO}	Maximum number of cells hardwired together that produce VFOs when somata are hyperpolarized
RA	Relative amplitude; amplitude divided by maximum amplitude observed
RA_{min}	Minimum relative amplitude observed

METHODS

For all our calculations, the electrotonic length is given by the formula for the generalized electronic distance in Goldstein and Rall (1974), which incorporates tapering. In this study, we denote the unit for one electrotonic length as λ.

3D Cell Reconstructions

We downloaded 3D cell reconstructions from NeuroMorpho.Org (Ascoli et al. 2007). All cell reconstructions are of pyramidal cells from the rat somatosensory cortex. The original studies for which the cells were reconstructed are as follows: Schubert et al. (2006); Shepherd and Svoboda (2005); Staiger et al. (2004); and Wang et al. (2002). We used 156 cells in total, 40 cells from layers 2/3, 59 cells from layer 4, and 57 cells from layer 5. After we downloaded the reconstructions, we translated them into NEURON (Carnevale and Hines 2006) using Cvapp. (Some corrections were made to the code for neurons with long processes.) In NEURON, we inserted currents and ran the simulations described below. We analyzed geometric information such as the diameter of the soma and all axonal processes in NEURON, MATLAB, and Apple Numbers '09. The width of the axonal arbor was computed with L-measure (Scorcioni et al. 2008).

In each 3D reconstruction, we measured the IS diameter (d_{IS}), the main axon diameter (d_{MA}), the ratio between the diameter of the soma and d_{IS} (s_{ratio}), and the electronic length of the sharp taper from the soma to the IS (ℓ_c). The cell reconstructions consisted of connected compartments, where each compartment was described by a list of diameters and locations. We define the main axon (or axonal trunk) as the sequence of connected compartments with the highest average diameter. We define d_{IS} as the first diameter listed below the soma that is <5 μm. We define d_{MA} as the smallest diameter listed between the soma and first collateral, i.e., the smallest diameter listed in the first axonal compartment in NEURON. In each reconstruction, the soma had only one diameter (d_S). We therefore set $s_{ratio} = d_S/d_{IS}$. We set ℓ_c as the electronic length between the point where the IS meets the soma as defined in NEURON and the point where the diameter reaches d_{IS}.

Simulations for AP Propagation Across Gap Junctions

We hypothesize that gap junctions may be present on any length of unmyelinated axon. Axons are unmyelinated on the IS, on the main axon for some distance below the IS (Palmer and Stuart 2006; Shu et al. 2007a; Sloper and Powell 1979) and on many collaterals (Salin et al. 1995; Schubert et al. 2006; Sloper and Powell 1979). Therefore, we use simulations to investigate how well the somatic voltage can control AP propagation across gap junctions in the IS, main axon, and collaterals.

To investigate AP propagation across gap junctions on the IS and main axon, we used simplified axon models with dimensions based on geometric measurements of the 3D cell reconstructions. As shown in Fig. 2, the simplified axon has a cylindrical soma and main axon, while the IS has a linear sharp taper from the soma followed by a linear shallow taper. There are three simplified axon models: one for layers 2/3, one for layer 4, and one for layer 5. All of them have the same structure but different dimensions, given in Table 1.

The main axon is 12-λ long with diameter d_{MA} given in table 1. The IS is 40-μm long. The d_{IS} in Table 1 is the diameter of the axon between the sharp and shallow tapers in the IS. The electrotonic length of the sharp taper is ℓ_c, which determines its length in micrometers (l_c). The length of the shallow taper is $(40 - l_c)$. The diameter of the soma is $d_s = d_{IS} \times s_{ratio}$, where s_{ratio} is given in Table 1. The length of the soma is the same as the diameter.

In NEURON, we took the geometry defined above and inserted Hodgkin-Huxley type leak, fast *Na*, and delayed rectifying *K* conduc-

Table 1. *Dimensions of simplified axon models*

	d_{MA}		d_{IS}		s_{ratio}		ℓ_c	
Layer	Means ± SD	Model	Means ± SD	Model	Means ± SD	Model	Means ± SD	Model
2/3	0.598 ± 0.105	0.6	1.234 ± 0.351	1.2	14.883 ± 5.877	14	0.015 ± 0.003	0.015
4	0.601 ± 0.135	0.6	1.569 ± 0.394	1.5	11.238 ± 2.999	11.2	0.015 ± 0.002	0.015
5	1.125 ± 0.323	1.2	2.205 ± 0.716	2	11.391 ± 3.774	11.4	0.02 ± 0.012	0.02

Data are means and SD of *1*) the main axon diameter (d_{MA}), *2*) the initial segment (IS) diameter (d_{IS}), (3) the ratio between the somatic diameter and IS diameter (s_{ratio}), and (4) the electrotonic length of the sharp taper from the soma to the IS (ℓ_c) of the cell reconstructions downloaded from NeuroMorhpo.org. Approximate values used in the simplified axon models are listed. See GLOSSARY for definitions.

tances from the layer 5 pyramidal cell axon in Traub et al. (2005a) or the conductances from Schmidt-Hieber et al. (2008) into all axonal compartments. In the axon model for layers 2/3 and 4, the conductances from Traub et al. (2005a) resulted in $\lambda \approx 122$ μm in the main axon, while $\lambda \approx 173$ μm in the main axon of the layer 5 axon model. For the conductances in Schmidt-Hieber et al. (2008), one electrotonic length is equivalent to ≈ 576 μm in the layer 2/3 and 4 models and ≈ 814 μm in the layer 5 model. In all models, the length of the main axon was well over 300 μm, the longest length of unmyelinated main axon reported thus far (Palmer and Stuart 2006; Shu et al. 2007a; Sloper and Powell 1979). However, we focused on the first 300-μm below the soma in our simulations. The voltage equation for these conductances is

$$C\frac{dV}{dt} = g_L(V_L - V) + g_{Na}m^3h(V_{Na} - V) + g_K n^4(V_K - V)$$

where m, h, and n are determined by equations of the form

$$\frac{dz}{dt} = \frac{z_\infty(V) - z}{\tau_z(V)}.$$

With the conductances from Traub et al. (2005a), the default sodium and potassium conductance are $g_{Na} = g_K = 0.45$ S/cm^2 in the IS, while the default conductances in the main axon are $g_{Na} = g_K = 0.2$ S/cm^2. We set the default g_{Na} in the main axon to be significantly lower because the sodium conductance decreases drastically beyond the IS in neocortical axons experimentally (Boiko et al. 2003; Kole et al. 2008; Lorincz and Nusser 2008). Unmyelinated axons are known to have a uniform sodium conductance in experiment (Waxman et al. 1995), so the IS and the main axon have uniform g_{Na} in our model. The passive parameters are as follows: $g_L = 1 \times 10^{-3}$ S/cm^2, $C = 0.9$ μF/cm^2, $V_L = -70$ mV, $V_{Na} = 50$ mV, $V_K = -95$ mV, and axial resistivity is 100 Ω-cm. The spiking conductances from the model in Schmidt-Hieber et al. (2008) yielded a different AP shape and much longer electrotonic length. The default conductances while using these conductances were $g_{Na} = g_K = 0.096$ in the IS and $g_{Na} = g_K = 0.03$ in the main axon.

The only current we inserted into the soma is a leak current, $g_L(V_s - V)$. To model all currents and synapses affecting the somatic voltage, we set the somatic leak conductance to $g_L = 2 \times 10^{-3}$ S/cm^2 and varied the somatic leak reversal potential V_s as a parameter.

A gap junction between two axons, A and B, at distance x μm from the soma was modeled by inserting the current $g_{gj}(V_{B,x} - V_{A,x})$, x μm away from the soma in axon A, and $g_{gj}(V_{A,x} - V_{B,x})$, x μm away from the soma in axon B. Assuming that the distance of the gap junction from the soma in the sending axon does not affect AP propagation too much, we always placed gap junctions at the same distance from the soma in each axon.

Note that while V_s and the distance between the gap junction and the soma are the same in both cells, the value of these parameters in the receiving cell largely determines whether APs will invade its axon. Therefore, this model applies to any connection where an AP crosses a gap junction into the IS or main axon, including APs propagating from gap junctions that connect a collateral onto the IS or main axon. We discuss the differences in the models used for IS and main axon gap junctions below.

IS gap junctions. As shown in Fig. 2, we tested AP propagation across a gap junction connecting the IS of two cells from the same layer, while varying the sodium conductance g_{Na} in the IS and the distance of the gap junction from the soma. When varying g_{Na}, we always kept $g_K = g_{Na}$ following Traub et al. (2005a). We stimulated the soma or distal main axon in one cell and tested for AP propagation in the neighboring cell. In the axon, we stimulated and tested for propagation $10\lambda \approx 1{,}730$ μm from the soma, so that the gap junction did not affect stimulation and there were no artifacts of a failed AP at the site where propagation was tested. Stimulations consisted of 3 nA for 1 ms in the soma or 2 nA for 0.3125 ms in the main axon applied 5 and 10 ms after the start of the simulation. We tested for AP propagation into the neighboring cell by checking if the voltage crossed the threshold $V_L + (V_{Na} - V_L)/3$ [approximately equal to -30 mV for conductances from Traub et al. (2005a)] at the distal end of the main axon. For $V_s = V_L - 10$, V_L, and $V_L + 10$ mV, and a range of values for g_{gj}, we found the threshold g_{Na} (g_{Na,V_s}) that allows AP propagation from one axon to the other. We also found the threshold g_{Na} where the main axon in the receiving cell fires twice, indicating that APs propagate successfully from both stimulations at 5 and 10 ms. For conductances from Traub et al. (2005a), we searched for g_{Na} thresholds only up to 2 S/cm^2. When APs did not propagate from one axon to another for $g_{Na} = 2$ S/cm^2, we set $g_{Na,V_s} = 2$ S/cm^2. Likewise, for conductances from Schmidt-Hieber et al. (2008) the maximum g_{Na} was 1 S/cm^2.

Main axon gap junctions. We then placed a gap junction on the main axons of two cells from the same layer, varying g_{Na} and the electrotonic distance of the gap junction from the IS (see Fig. 2). We stimulated the distal main axon of one cell and tested for AP propagation in the neighboring cell in the same manner as above. We did not stimulate the soma since the gap junction was relatively far from the soma and APs propagating to the gap junction from either location were similar. We kept g_{Na} at the default value in the IS and varied g_{Na} in the main axon. For $V_s = V_L - 10$, V_L, and $V_L + 10$ mV, and a range of values for g_{gj}, we found the threshold g_{Na} (g_{Na,V_s}) that allows AP propagation from one axon to another. Likewise, we also found the threshold g_{Na} where the main axon in the receiving cell fires twice, indicating that APs propagate successfully from both stimulations. As in the simulations for the IS, we searched for g_{Na} thresholds only up to 2 S/cm^2 for Traub et al. (2005a) conductances and 1 S/cm^2 for Schmidt-Hieber et al. (2008) conductances. However, sometimes the axon intrinsically fired when g_{Na} was set to a high value. [The layer 5 axon model intrinsically fired when $g_{Na} \geq \sim 0.8$ S/cm^2 for Traub et al. (2005a) conductances.] In this case, we only searched for threshold g_{Na} where the axon did not intrinsically fire.

Collateral Gap Junctions

Simulations testing AP propagation from axon collaterals were similar to simulations for the IS and main axon, with the following variations: to investigate AP propagation from collaterals into the main axon, we chose 11 representative 3D cell reconstructions, several from each layer. We did not choose any cells reconstructed for Shepherd and Svoboda (2005) because the authors kept track of only the 3D coordinates, not the diameter of axonal processes (G. M. Shepherd, personal communication). In NEURON, we took the exact geometry defined by the 3D cell reconstructions and inserted the same Hodgkin-Huxley type leak, *Na*, and *K* conductances as above into all axonal compartments. Only a leak conductance was inserted into the soma and dendrites.

We designated the first 40 μm below the soma as IS. Since the NEURON compartment for the soma was often less than a few micrometers long, we designated the soma compartment and any length of dendrite adjacent to it with a diameter ≥ 5 μm as "soma" when setting the leak conductance.

For each cell, we stimulated different collaterals and tested for AP propagation in the main axon as shown in Fig. 2. In each cell, we stimulated all collaterals at least 2/3 λ long, since APs could be initiated in those collaterals independently from the main axon. We stimulated collaterals at least 2/3 electrotonic lengths away from the main axon, so that the collateral at the stimulation site and main axon could fire independently. This excluded some collaterals that were too short electrotonically.

By varying g_{Na} throughout the axon below the IS, we found the threshold g_{Na} (g_{Na,V_s}) that allows propagation from the stimulation site on the collateral to the propagation site in the main axon. As in the simulations for the IS and main axon, we found g_{Na,V_s} for several values of V_s and for AP propagation for two stimulations within 5 ms.

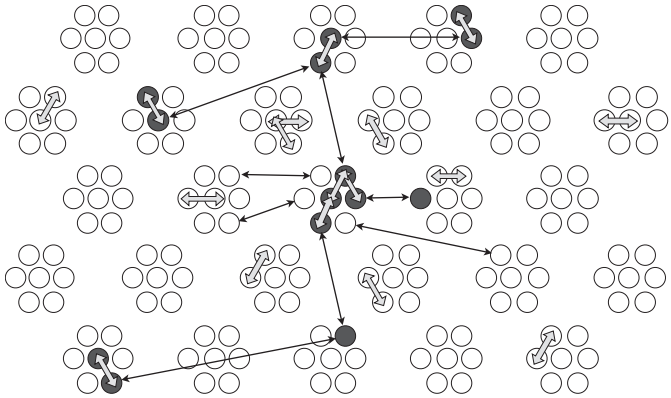

Fig. 3. Gap junction network. Cells are arranged in minicolumns which are placed on a hexagonal grid. Open arrows stand for IS and main axon gap junctions while filled arrows stand for collateral gap junctions. Gray cells form a connected cluster.

Gap Junction Network

Since our simulation results indicated that some cells may be hardwired together, we developed and analyzed a graph-theoretical network to investigate how many cells, on average, can be connected without cycles forming, as the probability of connecting increases (see Fig. 3.) We chose weights for the cells uniformly from the total axon lengths of the 3D cell reconstructions from layer 5. The cells were then grouped into columns with n_{cc} cells each and placed on a 90 $\times$ 30 hexagonal grid (Buxhoeveden and Casanova 2002; Feldman and Peters 1974; Mountcastle 1997 2003; Rakic 2008; Rockland and Ichinohe 2004). Based on the average axonal width of the cell reconstructions (540 μm) and a minicolumn width of 30 μm, we connected only cells that lay within $r_c = 9$ units (the distance between 2 columns is 1 unit) of each other on the hexagonal grid. Each pair of cells within r_c of each other on the hexagonal grid were connected with probability $1 - e^{-pL_1L_2}$, where p is the probability that two axons will form a gap junction per micrometer squared, L_1 is the total length of the first axon, and L_2 is the total length of the second axon. (The probability of 2 cells connecting is derived in APPENDIX C.) Since p is not known experimentally, we varied p from 0 to $p_4 = 4/(L^2M)$ where L is the mean weight of all cells and M is the number of cells within r_c of a single cell. The p_4 is the value of p that would yield an average of 4 connections per cell in an unweighted Erdös/Renyí random graph (Erdös and Renyí 1960). (See APPENDIX C for the calculation.) Since IS and main axon connections may also hardwire cells together, we also connected cells randomly within columns with a connection probability of p_{intra}. We set p_{intra} =5% per pair (Wang et al. 2010) to account for the maximum percentage of cells that could be hardwired together by IS and main axon connections, or we set $p_{intra} = 0$ per pair to investigate behavior when only collateral gap junctions hardwire cells together.

For each value of p, we generated 10 networks and numerically calculated the size of the largest cluster and number of cycles in each network. We computed the mean size of the largest cluster (n) and the mean number of cycles in the network (m_{cy}) over all 10 networks for each p. Both n and m_{cy} increase monotonically as p increases. We define the lowest value of p where $m_{cy} \geq 1$ as p_{cy}. Then, we set n_{cy} as the value of n when $p = p_{cy}$.

Computational Aspects

All NEURON simulations were run on the katana cluster at Boston University. We used the implicit Euler method with a time step of 0.001 ms for each simulation. Compartments were discretized into $\sim$1-μm pieces for models using the exact geometry of the cell reconstructions as well as simpler geometries. All code may be accessed at ModelDB (Accession No. 136309) (Hines et al. 2004).

RESULTS

Geometric Properties of 3D Cell Reconstructions

The main result of this section is the average dimensions found in the 3D cell reconstructions. We obtained 156 3D cell reconstructions from all neocortical layers of rat somatosensory cortex (see METHODS). Several geometric features of these reconstructions specified the dimensions of the simple axon model to simulate gap junctions on the IS and main axon, as shown in Fig. 2. Table 1 lists these parameters along with the dimensions actually used in our simple axon model (see METHODS).

A secondary result is the geometric ratio between branch points in the axon. We performed simulations using the exact geometry of the 3D reconstructions to test AP propagation from collaterals into the main axon. AP propagation through a branch point is determined by the geometric ratio between the parent branch the AP is propagating from and the daughter branches the AP is propagating to (Debanne 2004). Because we are concerned with antidromic AP propagation from putative gap junctions on collaterals into the rest of the axon, we computed the antidromic geometric ratio of branch points along collaterals as well as from collaterals into the main axon. Figure 4 shows that most branch points within collaterals have a geometric ratio of 2, where all branch diameters are the same. The antidromic geometric ratio from a collateral into the main axon can be much higher.

Somatic Voltage Can Control AP Propagation Across Gap Junctions in the IS and Main Axon

The somatic voltage of a pyramidal cell can control whether APs invade the axon from gap junctions if *1*) APs invade the axon when the somatic voltage is high, and *2*) APs are blocked when the somatic voltage is low. A number of parameters besides the somatic voltage come into play when considering whether an AP can propagate across the gap junction or not. These include the gap junction conductance (g_{gj}) and the excitability of the axon. Since the sodium conductance (g_{Na}) in neocortical pyramidal cell axons is largely unknown and is directly related to the excitability of the axon, we investigated

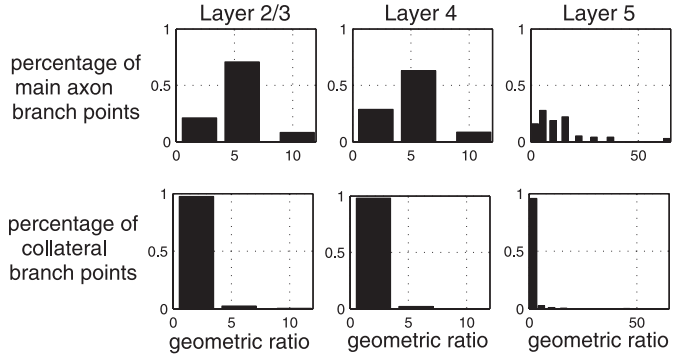

Fig. 4. Antidromic geometric ratios are highest where collaterals meet the main axon. We measured the antidromic geometric ratio from each collateral branch toward the soma. (Tapering within compartments was not substantial in collaterals, and the geometric ratio for tapering within a compartment is poorly defined.) *Top*: antidromic geometric ratio vs. the percentage of branch points from a collateral into the main axon with that geometric ratio. *Bottom*: antidromic geometric ratios of branch points within a collateral. Geometric ratio is 2 when all 3 branches at a branch point have the same diameter. In each layer, the percentage of branch points with geometric ratios >2 is much higher at the main axon vs. within collaterals.

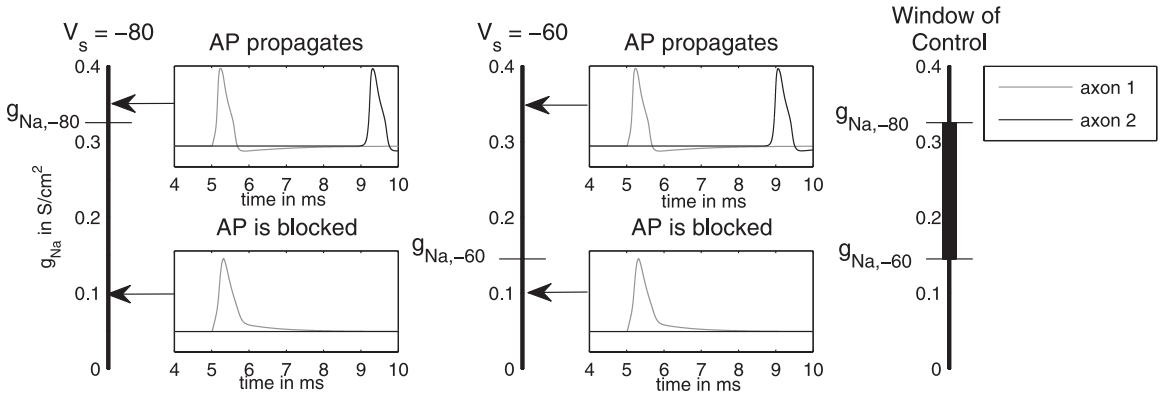

Fig. 5. Definition of window of control. Layer 5 simplified axon model, g_{gj} = 6 nS, gap junction is 213 μm from soma (1 λ below the IS). When $V_s = -80$ mV, APs propagate across the gap junction as long as $g_{Na} \geq g_{Na-80} \approx 0.325$ S/cm^2. When $V_s = -60$, APs propagates across the gap junction for $g_{Na} \geq g_{Na,-60} \approx 0.145$ S/cm^2. The window of control is the range of g_{Na} between $g_{Na},_{-60}$ and $g_{Na},_{-80}$.

the ranges of both g_{Na} and g_{gj} which allow for somatic voltage control over AP propagation. We consider somatic voltage control to be feasible physiologically if the ranges of g_{Na} and g_{gj} in which we have control are wide and are within physiological limits.

AP propagation across IS and main axon gap junctions. To investigate AP propagation across gap junctions in the IS and main axon, we simulated simplified axon models for layers 2/3, 4, and 5 using the spiking conductances from the pyramidal cell axons in Traub et al. (2005a). The dimensions of the axon models are based on measurements of the 3D cell reconstructions, given in Table 1. Gap junctions connected two axons from the same layer together at the same distance from the soma on either the IS or the main axon. As shown in Fig. 2, we stimulated one cell and then tested for AP propagation in the distal axon of the neighboring cell.

We varied two parameters in each set of simulations: V_s and g_{Na}, both of which affected the excitability of the axon. A high value of V_s raised the voltage in the axon according to electrotonic length, making the axon more excitable. A low V_s reduced the voltage in the axon making it less excitable (Shu et al. 2006, 2007b; Tuckwell 1988). When the gap junction was in the IS, we varied g_{Na} in the IS while keeping g_{Na} in the main axon fixed at the default conductance. When the gap junction was in the main axon, we varied g_{Na} in the main axon while keeping g_{Na} in the IS fixed. APs did not propagate across a gap junction when g_{Na} was low, even for high values of V_s.

Definition of window of control. For a fixed value of g_{Na}, we say that the somatic voltage controls AP propagation across a gap junction if *1*) APs propagate across the gap junction when $V_s = -60$ mV, and *2*) APs do not propagate across the gap junction when $V_s = -80$ mV. The window of control for a gap junction is the range of g_{Na} values for which the somatic voltage controls AP propagation from that gap junction. We calculated the boundaries of the window of control by fixing V_s at -80 or -60 mV and then finding the value of g_{Na} (g_{Na,V_s}) where APs can propagate from one axon to another if $g_{Na} \geq g_{Na,V_s}$. Since g_{Na} does not have to be as high for AP propagation when $V_s = -60$ vs. $V_s = -80$, the somatic voltage can control AP propagation if $g_{Na},_{-60} \leq g_{Na} \leq g_{Na},_{-80}$ (see Fig. 5).

Windows of control for gap junctions on the IS. Figure 6 shows results for gap junctions on the IS in the layer 5 model

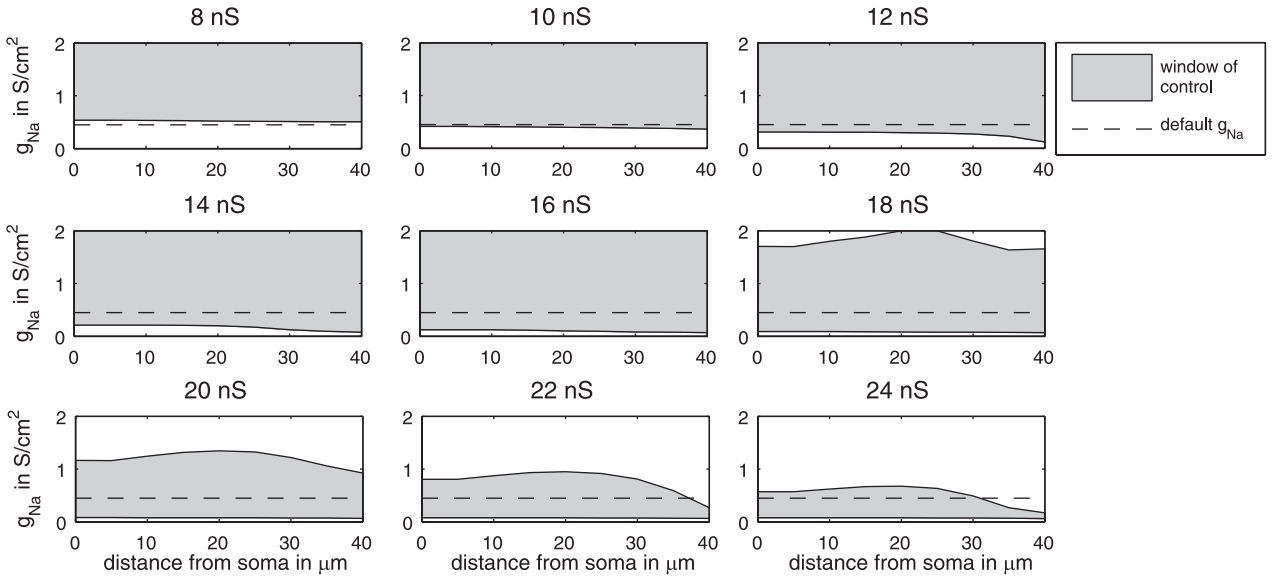

Fig. 6. Windows of control are wide for a range of gap junction conductances when the gap junction is in the IS. Layer 5 model, distal axon is stimulated. The default sodium conductance in the IS, g_{Na} = 0.45 S/cm^2, is plotted as a baseline in all panels. The window of control contains the default g_{Na} for g_{gj} = 10 to 24 nS. Note: the maximum g_{Na} we searched was 2 S/cm^2.

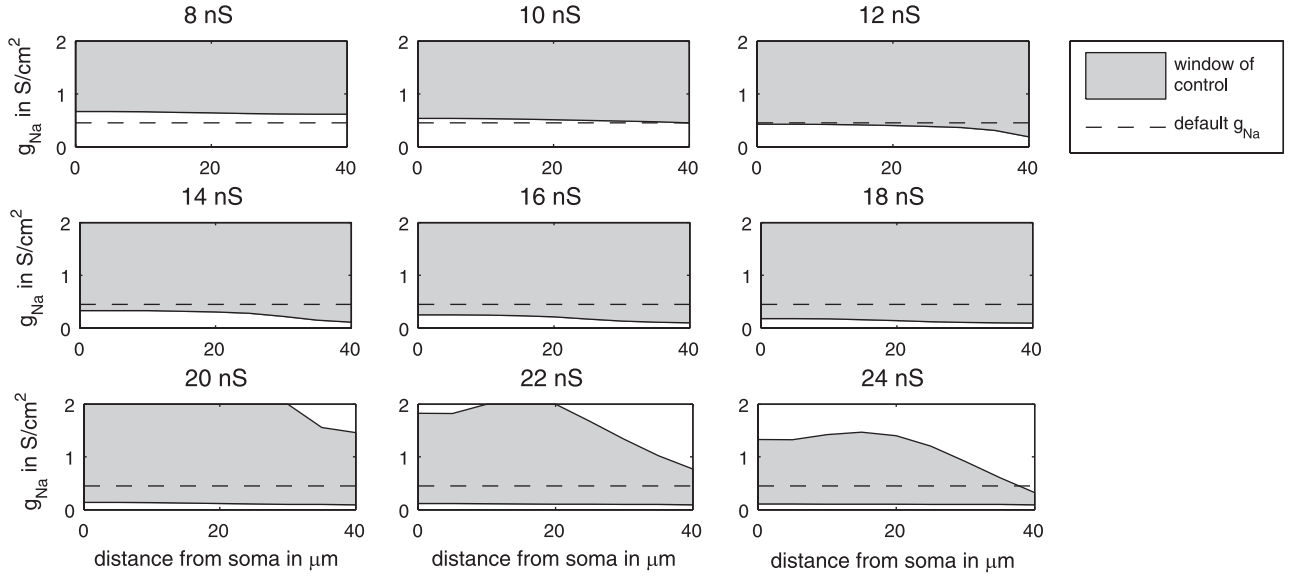

Fig. 7. Windows of control get larger as input resistance decreases, and shift up slightly. Here, the somatic leak conductance is $g_L = 3 \times 10^{-3}$ S/cm^2 instead of $g_L = 2 \times 10^{-3}$ S/cm^2. Gap junction on the IS, distal axon was stimulated. Default value of $g_{Na} = 0.45$ S/cm^2 is plotted as a baseline. In our model, the default somatic leak conductance of $g_L = 2 \times 10^{-3}$ corresponds to an input resistance of ~26 MΩ, which is comparable to input resistances reported during the down-state of slow-wave sleep and rapid eye movement sleep without ocular saccades (Steriade et al. 2001). The somatic leak conductance $g_L = 3 \times 10^{-3}$ yields an input resistance of ~18.6 MΩ in our model, which is comparable to input resistances seen during the up-state of slow-wave sleep and during ocular saccades in rapid eye movement (Steriade et al. 2001).

and conductances ranging from 8 to 24 nS. The window of control is very wide for $g_{gj} = 8$ nS through $g_{gj} = 18$ nS. For $g_{gj} = 10$ through 24 nS, the default IS sodium conductance, $g_{Na} = 0.45$ S/cm^2, is within the window of control for almost the entire IS. Above 24 nS, the window of control falls below the default g_{Na} in the IS. These values of g_{gj} fall within the range of gap junction conductances reported in Wang et al. (2010). [See APPENDIX A for an analysis on how these results compare to Wang et al. (2010).] Therefore, for a wide range of physiological g_{gj} and g_{Na}, gap junctions can be controlled by the somatic voltage. Windows of control shifted slightly when the gap junction was on the IS and the soma was stimulated instead of the distal axon. The windows of control were wider and shifted up slightly when the somatic leak conductance was set to $g_L = 3 \times 10^{-3}$ S/cm^2 instead of $g_L = 2 \times 10^{-3}$ (see Fig. 7).

Windows of control for gap junctions on the main axon. Figure 8 shows windows of control for gap junctions on the main axon using the layer 5 axon model. The default conductances of 0.45 S/cm^2 for the IS and 0.2 S/cm^2 for the main axon are shown as a baseline. As g_{gj} rises, the window of control

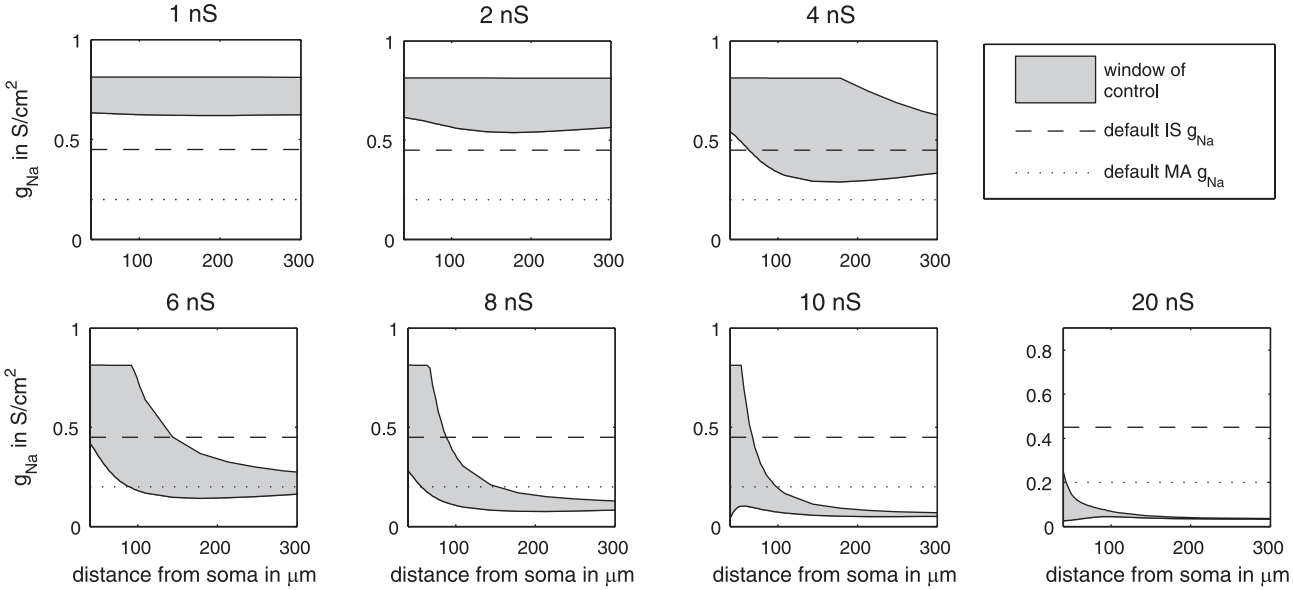

Fig. 8. Windows of control for main axon gap junctions are wide for several gap junction conductances and distances from the soma. Layer 5 simplified axon model. Default g_{Na} conductances for the IS and MA are shown. The window of control in the main axon opens, shifts to lower g_{Na} values, and then closes as distance from the soma and g_{gj} increase. Close to the IS, the window of control is wide for $g_{gj} = 6$ to 10 nS. Farther from the IS, the window of control is wide for $g_{gj} = 4$ to 8 nS. Since the longest unmyelinated distance below the soma is reported to be is 300 μm (Shu et al. 2007a), there is a wide range of g_{Na} in which AP propagation can be controlled where most main axons are unmyelinated.

opens and then moves down to lower values of g_{Na} and closes. As the gap junction moves farther away from the soma, the window of control tends to shift down within the first 100 μm from the soma (60 μm from the IS) and then tapers, centering on a particular value of g_{Na}. Close to the soma, the window of control is wide for higher values of g_{gj}, while the window of control is wide for lower values of g_{gj} far from the soma. This suggests that g_{gj} must shift to lower values for gap junctions farther from the soma, in order for the gap junction to stay within the window of control. It is possible that g_{gj} may smoothly taper with axon diameter. It could also be regulated by the cell to stay within the window of control (Goodenough and Paul 2009; Parker et al. 2009; Sutor and Hagerty 2005). Windows of control for the layer 2/3 and 4 simplified axon model behave similarly (results not shown).

Somatic voltage can control VFOs. According to Lewis and Rinzel (2000) and Munro and Börgers (2010), VFOs are generated by expanding waves of APs propagating throughout the axonal plexus. Each period of the oscillation is produced by an expanding wave. Therefore, an axonal plexus can produce VFOs at 200 Hz if successive waves of APs may propagate across gap junctions within 5 ms of each other. We therefore calculated the threshold g_{Na} to allow two APs to propagate across a gap junction within 5 ms (g_{Na,VFO,V_s}) as well as the threshold g_{Na} for AP propagation (g_{Na,V_s}). Figure 9 shows the VFO window of control for g_{gj} =6 nS: i.e., the range of g_{Na} values for which a depolarizing somatic voltage allows multiple APs to propagate across a gap junction at VFO frequencies, while a hyperpolarizing somatic voltage disables propagation completely. This means that the somatic voltage can enable or disable VFOs, as seen in experiment (Grenier et al. 2001).

Somatic spikelets. In our simulations, when APs propagated across a gap junction, they proceeded antidromically to the soma to produce either a full spike or spikelet. Sometimes, when an AP failed to cross a gap junction in the IS, a spikelet could still be seen in the soma because it was very close to the gap junction. Figure 10 shows that spikelets produced by APs failing to enter the soma either from an IS gap junction or antidromically looked very similar.

Results are robust with respect to membrane conductances. Simulations using the Hodgkin-Huxley type conductances from Schmidt-Hieber et al. (2008) instead of Traub et al. (2005a) yield similar results (results not shown).

Somatic Voltage Cannot Control AP Propagation from Axon Collaterals in Our Model

We hypothesize that the somatic voltage does not greatly affect propagation across gap junctions far away from the soma on collaterals. If this is the case, then APs in a given collateral always propagate or never propagate across a gap junction on the collateral. Once an AP crosses a gap junction in a collateral, it must propagate antidromically along the collateral into the main axon to reach axon terminals and other gap junctions in the axon. In our 3D cell reconstructions, over all branch points on a given collateral branch, the largest geometric ratio tends to be between the collateral and the main axon as shown in Fig. 4. Since AP propagation down neocortical axons is reliable (Cox et al. 2000), and the diameters of the different branches meeting at one point is often the same, we expect APs to reliably propagate up axon collaterals as well. Therefore, an AP propagating antidromically up a collateral branch is most likely to fail at the branch point where the collateral meets the main axon. This means that the somatic voltage of a cell could control APs propagating from gap junctions on collaterals by blocking AP propagation from the collateral into the main axon.

Windows of control for AP propagation from axon collaterals. To test the idea of controlling propagation from collaterals, we simulated model axons having the exact geometry of the 3D cell reconstructions, stimulating collaterals and testing for a propagated AP in the main axon (see Fig. 2) The values of $g_{Na,\ V_s}$ and the geometry of the cell determined whether an AP

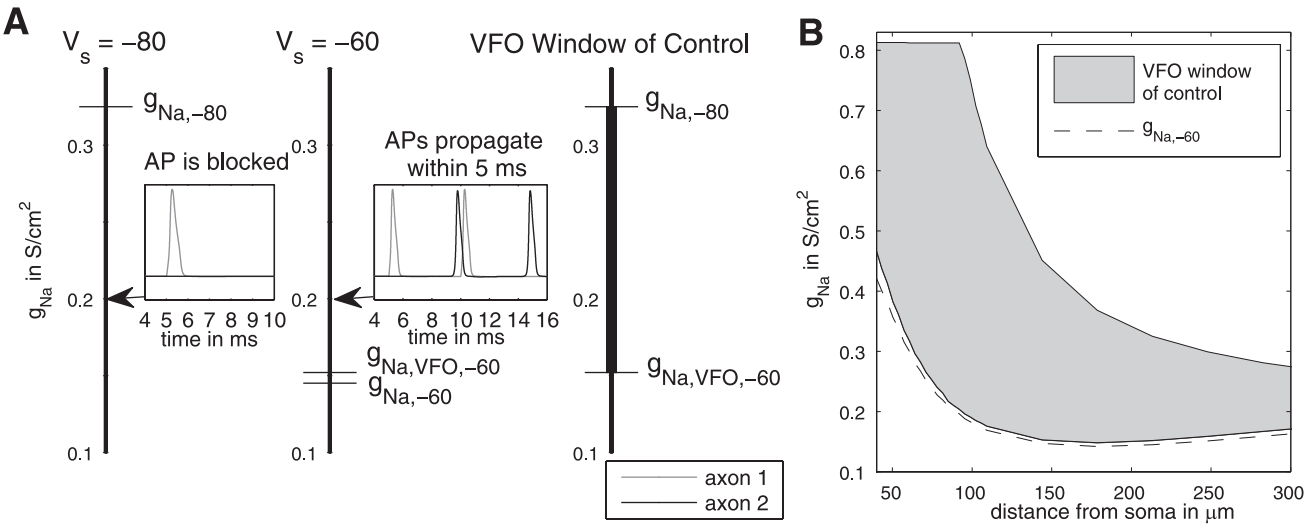

Fig. 9. Somatic voltage can control very fast oscillations (VFOs) in an axonal plexus. Layer 5 simplified axon model, g_{gj} = 6 nS. *A*: definition of VFO window of control. Gap junction is 213 μm from the soma. VFO window of control is the range of g_{Na} values where $g_{Na,VFO,-60} \leq g_{Na} \leq g_{Na,-80}$, so that APs may propagate across the gap junction within 5 ms of each other when *Vs* = −60 and all APs are blocked when V_s = −80. B: VFO window of control is close to the window of control for AP propagation. The VFO window of control is shown alongside g_{Na}, −60, which marks the lower boundary for the window of control for AP propagation. Since $g_{Na,-60}$ and $g_{Na,VFO,-60}$ are close together, the somatic voltage may also control VFOs for a wide range of g_{Na}.

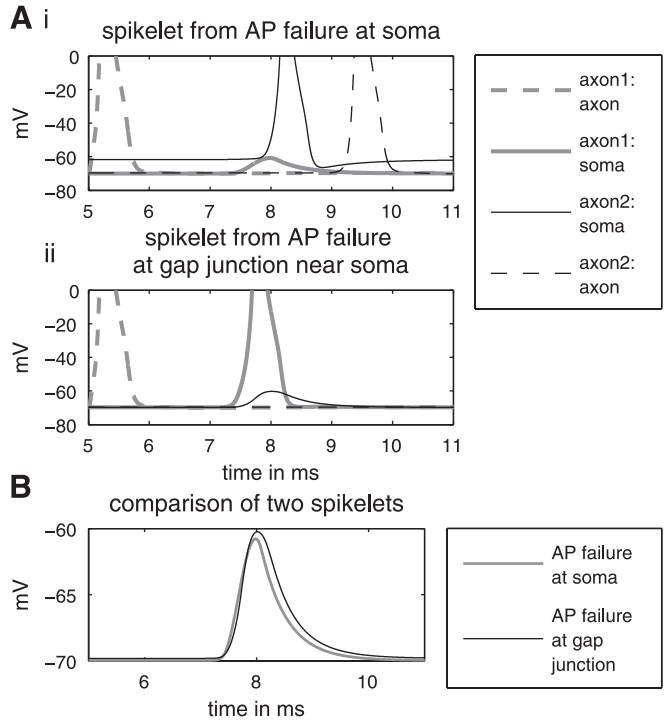

Fig. 10. Comparison of spikelets from propagation failure at the soma or at the gap junction near the soma. Layer 5 simplified axon model, default sodium conductances. *A*, *i*: length of the soma is 10 times the normal length in axon 1 so that APs fail to invade the soma in axon 1. Gap junction is 173 μm from the IS, $g_{gj} = 6$ nS. Note that while the gap junction is relatively close to the soma, the recording site in the axon is 1,730 μm away from the soma. Therefore, APs and spikelets appear in the soma of the receiving cell before the axon. While APs fail at the soma in axon 1, APs propagate across the gap junction into axon 2 because $V_s = -60$ mV. *A*, *ii*: both axons have default sized somata. Gap junction is 20 μm from the soma with $g_{gj} = 10$ nS, and $V_s = -70$. While APs cannot cross the gap junction, a spikelet can be seen in the soma of axon 2 because the gap junction is close to the soma. *B*: 2 spikelets from *A*, *i* and *A*, *ii* on top of each other. One can see that their amplitudes and time course are nearly identical.

propagated from the collateral into the main axon. In 11 representative 3D cell reconstructions, we calculated the threshold $g_{Na}(g_{Na,V_s})$ at which APs propagate from points on the axon collaterals into the main axon. Figure 11 shows the windows of control for points on the axon collaterals in these 11 representative cells, i.e., the range of g_{Na} where $g_{Na,-60} \leq g_{Na} \leq g_{Na,-80}$.

In Fig. 11, we see that windows of control vary significantly. Windows of control do not overlap between different cells, nor do they overlap for different collaterals in the same cell. The window of control may even be different for the same collateral if it is stimulated in a different location (see the windows of control marked by filled diamonds in Fig. 11). We obtained similar results using Hodgkin-Huxley type conductances from Schmidt-Hieber et al. (2008) instead of Traub et al. (2005a). (Results not shown.) Therefore, there is no single value of g_{Na} for which the somatic voltage can effectively control AP propagation from all collaterals simultaneously.

How Many Uncontrollable Connections Could There Be?

In the above section, we showed that the somatic voltage may not control AP propagation from collaterals. The somatic voltage may not control AP propagation across some gap junctions found in the IS or main axon either. Here, we address: how many cells could be hardwired together by uncontrollable connections? Recall that two cells are hardwired together when APs propagate from one cell's axon to the other's regardless of somatic voltage. In other words, two cells are hardwired together if their axons are connected by a gap junction and g_{Na} is above the window of control in the axon of one of the cells. A neocortical axonal plexus may produce many unwanted spikes if too many cells are hardwired together. On the other hand, the somatic voltage may effectively control APs propagating through the axonal plexus if only a small percentage of cells are hardwired together. Below, we estimate the number of cells hardwired together and show that the percentage of cells hardwired is small compared with the size of the network.

To estimate how many cells may be hardwired together in the neocortex, we consider the number of pyramidal cell axons that an AP can travel through when somata are hyperpolarized and all controllable connections are blocked. Uniform somatic hyperpolarization is most easily achieved during the slow-oscillation seen during anesthesia or slow-wave sleep. Moreover, VFOs seen during the upstate of the slow oscillation are greatly reduced during the down-state. This suggests that APs can propagate through controllable gap junctions during the up-state and cannot during the down-state of the slow oscillation. To estimate the number of cell axons APs may propagate through during the down-state, we compute two separate bounds: one for cell clusters producing VFOs when somata are hyperpolarized (N_{VFO}) and another for cell clusters that are not producing VFOs (N_{O}). Since we are concerned with cluster sizes, and a cell cannot both be in a cluster that is producing a VFO and not producing a VFO, our constraint is $\max(N_{\mathrm{VFO}}, N_{\mathrm{O}})$.

Number of cells hardwired together that produce VFOs during somatic hyperpolarization. We estimated N_{VFO} based on the data presented in Grenier et al. (2001), which shows VFOs during the slow oscillation induced by ketamine-xylazine anesthesia. During these oscillations, the up-state and down-state of individual cells tend to be synchronized with the up and down states of the local field potential. Therefore, we may expect most somata to be hyperpolarized together during the down-state. Figure 5 of Grenier et al. (2001) shows the *RA* (the amplitude divided by the maximum amplitude observed) of VFOs vs. the somatic voltage of a single pyramidal cell during the slow oscillation. The relative amplitude is very low when somata are hyperpolarized but is not zero. If we assume that the VFO relative amplitude is above noise level, then how many cells could be participating in the VFO during the down-state? Here, we give a brief estimate of the number of cells generating a VFO during the down-state. A more thorough analysis is given in APPENDIX B.

The number of cells oscillating during the down state can be approximated by:

$$N_{\mathrm{VFO}} \approx RA_{min} \times m_{max}$$

where RA_{min} in the minimum RA observed and m_{max} is the number of cells generating the maximum VFO amplitude. In Grenier et al. (2001; Fig. 5), it appears that RA_{min} can be as high as:

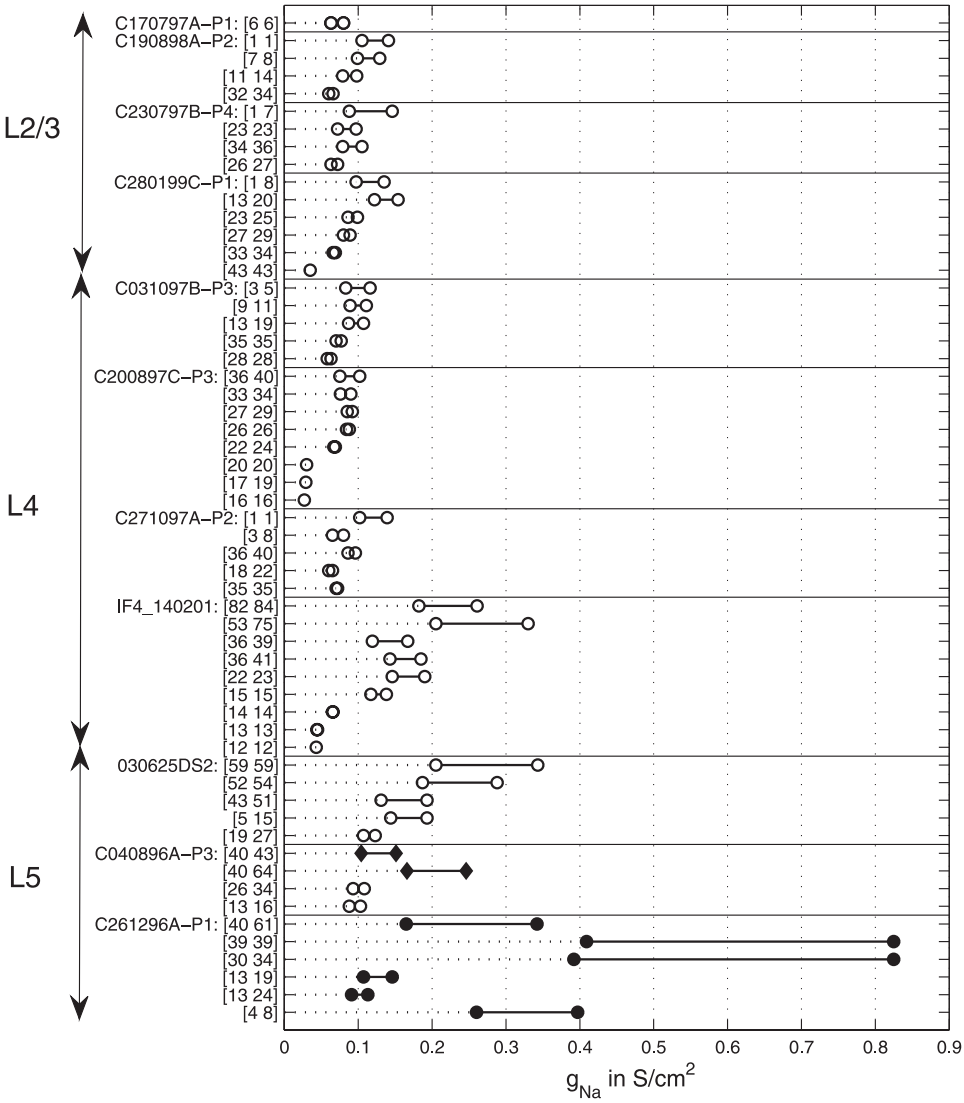

Fig. 11. Windows of control for AP propagation from a collateral into the main axon. Cells are organized according to the cortical layer they originated from. Each cell is identified by it's name on neuromorpho.org. Each collateral is marked with 2 numbers: [*m n*], where *m* is the NEURON number of the first collateral compartment and *n* is the NEURON number of the compartment that was stimulated. Collaterals are listed according to their distance from the soma: closer collaterals are listed first. Windows of control for the last cell "C261296A-P1" are marked with filled circles. Windows of control for the collaterals with $m = 39$ and $m = 30$ are both approximately [0.4, 0.82] S/cm^2. This means that the somatic voltage can control propagation from both of these collaterals if $g_{Na} \in [0.4, 0.82]$. However, the somatic voltage cannot control AP propagation from any of the other collaterals since their windows of control do not overlap [0.4, 0.82]. In general, windows of control often do not overlap for different collaterals in the same cell. There is even 1 example where the windows of control do not overlap for different stimulus locations on the same collateral (marked with filled diamonds).

$$RA_{min} \approx 0.01$$

which is the amplitude corresponding to a somatic voltage of approximately −83 mV. The number of cells generating the maximum VFO observed can be approximated by the number of pyramidal cells connected together in a large component of the axonal plexus generating the VFO. The depth electrodes in Grenier et al. (2001) were placed 0.8–1 mm underneath the pial surface, which should correspond to layer 5 according to Skoglund et al. (1996). While the depth electrodes were placed 1.5 mm apart in Grenier et al. (2001), their range is uncertain. However, activity generating the local field potential should fall within 1 mm^2 (Katzner et al. 2009). We therefore make the following estimates: *1*) number of cells in L5 under 1 mm^2: 23,000 (Skoglund et al. 1996); *2*) percentage of cells that are pyramidal in neocortex: approximately 85% (Beaulieu 1993); and *3*) percentage of pyramidal cells in a large cluster: 2/3 (Traub et al. 1999).

Assuming that pyramidal cells electrically couple only to cells in the same layer (Gutnick et al. 1985), $m_{max} \approx (2/3) \times 0.85 \times 23{,}000$ and

$$N_{\mathrm{VFO}} \approx 0.01 \times (2/3) \times 0.85 \times 23,000 \approx 130$$

Number of cells hardwired together that do not produce VFOs during somatic hyperpolarization. How many cells must be hardwired together to produce VFOs? There are two different mechanisms for VFOs in an axonal plexus (Lewis and Rinzel 2000; Munro and Börgers 2010). Externally driven VFOs can occur if hundreds of axons are connected together, and there is a small amount of external stimulation [a stimulation rate of 2/s/cell will suffice; Traub et al. (1999)]. Reentrant VFOs can occur if there are cycles in the network with unidirectional propagation block (Lewis and Rinzel 2000; Munro and Börgers 2010). Relatively few cells are required to form cycles for reentrant VFOs vs. the number of cells needed to form a connected cluster large enough to produce externally driven VFOs. Therefore, we calculated the average number of cycles (m_{cy}) in a graph-theoretical network (see METHODS). As the probability that gap junctions form increases, the average number of cycles (m_{cy}) also increases. Recall that n_{cy} is the average size of the largest cluster when $m_{cy} = 1$; On average, n_{cy} is the number of cells needed in a cluster to form a cycle.

The number of cycles in our network depends on the number of cells in a column (n_{cc}), which can range from 3 to 20 cells per minicolumn (Mountcastle 1997; Rockland and Ichinohe

2004). APPENDIX C shows that when $p_{intra} = 5\%$, n_{cy} is maximized when $n_{cc} = 3$, and when $p_{intra} = 0$, n_{cy} is maximized when $n_{cc} = 20$. Figure 12 shows that when $p_{intra} = 0$ and $n_{cc} = 20$, collateral connections will form a cycle when there are $n_{cy} \approx 70$ cells in the largest cluster. Similarly, $n_{cy} \approx 63$ when $p_{intra} = 5\%$ and $n_{cc} = 3$. This means there can be up to $N_O \approx 70$ cells connected together by uncontrollable gap junctions without producing a VFO.

Constraint on number of cells hardwired together. Above, we found that the maximum number of axons firing at VFO frequencies during somatic hyperpolarization is $N_{VFO} \approx 130$, based on assumptions of the numbers of cells generating the local field potential and relative amplitudes of VFOs. We also found that the number of cells that can be connected together without producing a VFO is $N_O \approx 70$. Since $N_{VFO} > N_O$, the constraint on the number of cells hardwired together is $N_{VFO} \approx 130$.

DISCUSSION

Our simulations show that the somatic voltage can control AP propagation across gap junctions in the IS and main axon of neocortical pyramidal cells over a wide range of physiologically plausible gap junction conductances (Wang et al. 2010), while the somatic voltage cannot effectively control AP propagation from collaterals into the main axon. Since the relative amplitude of VFOs falls to ~1% when cells are hyperpolarized, our computations suggest that at most ~130 cells are hardwired together, at least in layer 5. This indicates that the subthreshold somatic voltage of pyramidal cells can effectively control AP propagation from the axonal plexus into its main axon by controlling AP propagation across IS and main axon gap junctions.

Implications for Neocortical Computation

Our results imply that neocortical pyramidal cell somata do not themselves have to generate action potentials to send spikes to axon terminals; all they have to do is depolarize. A pyramidal cell with a depolarized somatic voltage will forward any spike that is received from the axonal plexus orthodromically to its axon terminals and antidromically toward the soma. A cell with a hyperpolarized soma will block signals propagating from the axonal plexus. Therefore, neocortical pyramidal cells can send signals to postsynaptic cells simply by controlling their subthreshold somatic voltage.

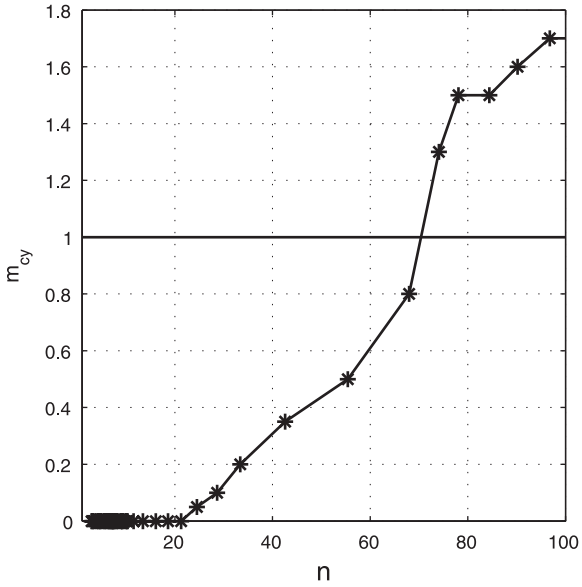

Fig. 12. Average number of cycles (m_{cy}) as a function of the mean size of the largest cluster (n) for $n_{cc} = 20$. Each data point gives (n, m_{cy}) for a single value of p. In our network model, as p increases, so do n and m_{cy}. Shown is that 1 cycle is expected when $n = n_{cy} \approx 70$. Therefore, reentrant VFOs are likely once the largest cluster size is >70.

Although we show that pyramidal cells are "hardwired" to at most $N_{VFO} \approx 130$ other pyramidal cells, the actual number of cells hardwired together may be much smaller. For instance, the constraint of 130 is based on the minimum relative amplitude $RA_{min} \approx 0.01$, which is an upper bound determined by visually inspecting the data in Grenier et al. (2001; Fig. 5). If we reduce N_{VFO} so that $N_{VFO} < N_O$, then the constraint on how many axons may be hardwired together is $N_O \approx 70$. However, this is also an overestimate, since it is based on minicolumns with the maximum number of axons in each column and a random network. Random networks tend to have a few larger clusters, while all other clusters are very small. The sizes of clusters in the neocortex may be more uniform. Even if 130 pyramidal cell axons are hardwired so that, once one of them fires, they all fire regardless of somatic polarization, this number is still small compared with an estimated total of 20,000 layer 5 pyramidal cells participating in an axonal plexus in 1 mm^2 of neocortex. While we are not able to estimate the number of hardwired cells in all cortical layers, our results suggest that there is little "random" activity in the axonal plexus, uncontrolled by somatic voltage.

Because neocortical pyramidal cells can send signals to postsynaptic cells merely by somatic polarization, we hypothesize that pyramidal cell subthreshold activity may be more important than previously thought. Thus, while spiking activity may appear sparse, cells may be sending many signals to postsynaptic cells (Brecht and Sakmann 2002; Crochet and Petersen 2006; Hromádka and Zador 2009; Margrie et al. 2002).

Spikelets may be an important form of subthreshold activity. Our simulations show a full AP or spikelet in the soma when an AP invades the main axon. A spikelet occurs if the AP fails to enter the main axon. This is in line with previous work connecting spikelets with axonal gap junctions in simulations (Draguhn et al. 1998) and experiment (Schmitz et al. 2001). This also agrees with experimental work in Mercer et al. (2006) where spikelets in a neocortical pyramidal cell lead to excitatory postsynaptic potentials in a postsynaptic cell. It is possible to see a somatic spikelet when no AP has invaded the main axon. In our simulations, we also saw spikelets when an AP fails to propagate across a gap junction that is close to the soma. Spikelets resulting from an AP failing to enter the soma antidromically or directly through a gap junction look very similar (as shown in Fig. 10). However, one may be able to detect the difference between these two conditions because junctions close to the soma may have a high coupling coefficient, as shown in Wang et al. (2010). In experiments, it is also possible to see spikelets from basal dendrites (Milojkovic et al. 2005). However, spikelets originating from basal dendrites lack the afterhyperpolarization seen in spikelets originating from axons (Schmitz et al. 2001). Therefore, studying spikelet and other subthreshold activity may give a broader picture of neocortical processing.

Cells can form assemblies simply by depolarizing together. Figure 3 (see METHODS) illustrates a cluster of cells connected by gap junctions. If all cells in the cluster depolarize together and one of them fires, then they all effectively fire as a unit. Depolarized cells form local cell assemblies on a millisecond time scale. Moreover, chemical synapses onto the soma and dendrites can affect neural processing by changing the subthreshold somatic voltage, while large assemblies may occur during synchronized up-states as seen in slow-wave sleep. In previous models of an axonal plexus (Lewis and Rinzel 2000, 2001; Munro and Börgers 2010; Traub et al. 1999), large networks of axons with a small amount of stimulation produce VFOs. Therefore, if a large group of cells depolarizes together, then their axons may produce VFOs, sending a tetanic signal to postsynaptic cells. Such large assemblies may be important for learning, as tetanic stimulation is associated with long-term potentiation (Teskey and Valentine 1998; Tsumoto 1990).

Because we can constrain the number of cells hardwired together by gap junctions, our results suggest that gap junction conductance is regulated so that AP propagation across gap junctions is controllable. Gap junctions are regulated in many ways in other parts of the brain and throughout the body (Goodenough and Paul 2009; Sutor and Hagerty 2005). It is even possible for a cell to regulate the coupling coefficient of a gap junction throughout its lifetime (Parker et al. 2009).

Implications for Epilepsy

In our model, AP propagation from gap junctions on collaterals cannot effectively be controlled by the somatic voltage. Thus, if gap junctions on collaterals form a cycle in the axonal plexus, then APs may propagate around that cycle regardless of somatic voltage. At the same time, APs can easily be blocked in one direction along a cycle where a collateral meets the main axon, as is illustrated in Fig. 13. Once there is an AP traveling in one direction along a cycle, it would generate reentrant VFOs that cannot be blocked by somatic hyperpolarization. These persistent reentrant VFOs would provide continual tetanic stimulation to postsynaptic cells, which may lead to epilepsy according to the kindling model (Bertram 2007).

Extra uncontrollable gap junctions may result from axonal sprouting (Salin et al. 1995) or lesions cut at certain angles (Gutnick et al. 1985). Animal models of posttraumatic epilepsy show extensive axonal sprouting (Pitkänen and McIntosh 2006; Salin et al. 1995). Temporal lobe epilepsy has been linked to lesions in the brain (Chang and Lowenstein 2003; Chevassus-au-Louis et al. 1999; Engel 1996; Salazar et al. 1985; Scharfman 2008). A close connection between fast ripples (VFOs >150 or 250 Hz, depending on the species) and temporal lobe epilepsy was shown experimentally in Bragin et al. (2002, 2004). Fast ripples may, in fact, be reentrant VFOs, as APs traveling around cycles in a network can generate very high frequency oscillations in simulations (Munro and Börgers 2010). Clinically, fast ripples and VFOs are associated with the seizure onset zone (Engel et al. 2009; Staba et al. 2004b; Traub et al. 2005b; Urrestarazu et al. 2007; Worrell et al. 2004, 2008) and seizure initiation (Grenier et al. 2003; Traub 2003; Traub et al. 2010). If lesions induce VFOs through axonal sprouting, then our results may explain why temporal epilepsy behaves similarly to the kindling model for epilepsy (Bertram 2007).

Relation to Other Work

Other studies on the effect of somatic voltage on AP propagation in axons include the following: Debanne et al. (1997); Munro and Börgers (2010); and Shu et al. (2006, 2007b). Our previous work (Munro and Börgers 2010) shows that the somatic voltage affects AP propagation across gap junctions in a simplified axon model. Shu et al. (2006, 2007b) show that somatic depolarization affects AP shape in the axon with respect to a slowly inactivating K^+ current with a time scale of 2.3 s. While AP shape influences propagation in general, these currents would not come into play in the axonal plexus unless cells are depolarized for a prolonged period of time, which is unlikely during normal neocortical processing and slow-wave sleep. Prolonged periods of depolarization may occur during seizures, and then these currents may influence activity in the axonal plexus. Experiments in Debanne et al. (1997) show that the history of the somatic voltage affects AP propagation in hippocampal pyramidal cells by means of an A-type potassium [$K(A)$] current. However, neocortical pyramidal cell axons are not reported to have a $K(A)$ current and AP propagation does not appear to be history dependent in neocortical pyramidal

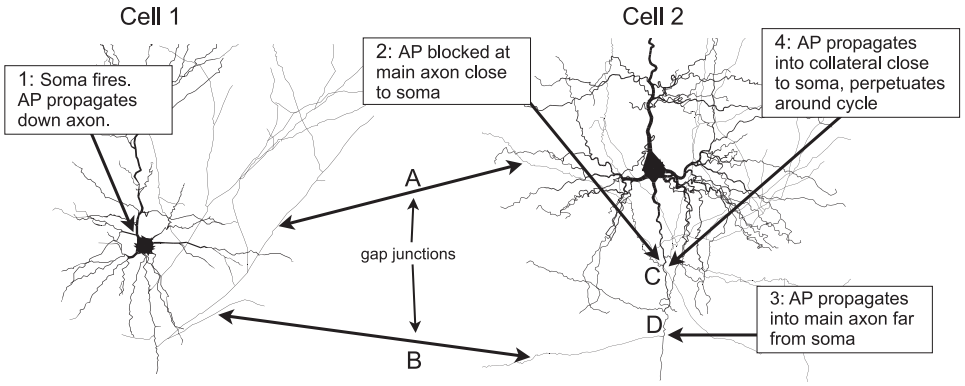

Fig. 13. Scenario showing how reentrant activity can occur when connections on collaterals form a 2-cell cycle. Above are 2 cell reconstructions. Scenario is as follows: *1*) *cell 1* fires and an AP travels down its axon and across the 2 gap junctions on its collaterals. *2*) AP propagating through gap junction *A* is ultimately blocked because the collateral at *C* is much thinner than the main axon. *3*) AP propagating through gap junction *B* invades the main axon of *cell 2* because the collateral and main axon at *D* are about the same size. Note that, if both APs invaded the main axon of *cell 2*, then they would annihilate each other. However, since the AP at *C* was blocked, *4*) the AP at *D* propagates up the main axon and into the collateral at C. This AP then continues to propagate into *cell 1* and around the cycle formed by the collaterals.

cells (Cox et al. 2000; Koester and Sakmann 2000; Shu et al. 2006).

All of our results are based on the geometry of neocortical axons and how they may be coupled together by gap junctions to form an axonal plexus. Since we based our models entirely on neocortical data, they may not apply to other areas of the brain. In particular, our results may not apply to the hippocampus, where the main axon may be unmyelinated for some distance below the soma and main axons as well as collaterals run roughly parallel to each other. Therefore, gap junctions connecting unmyelinated axons may be too far away from the soma to be controlled by the somatic voltage. In this arrangement, control may be mediated through other means.

While axonal gap junctions may explain the presence of VFOs, an alternative hypothesis is that VFOs are generated by synchronous firing of interneurons (Stacey et al. 2009; Ylinen et al. 1995). However, VFOs are unaffected when GABAergic transmission is blocked (Nimmrich et al. 2005; Roopun et al. 2010; Staba et al. 2004a), while they are consistently reduced by gap junction blockers (Cunningham et al. 2004; Nimmrich et al. 2005; Roopun et al. 2010). There is evidence that interneurons do not fire at VFO frequencies during VFOs (Roopun et al. 2010). Moreover, interneurons are most likely to synchronize at VFO frequencies though gap junctions formed by Cx36. However, when Cx36 is removed genetically, VFOs persist in vivo (Buhl et al. 2003; Hormuzdi et al. 2001) and in vitro (Hormuzdi et al. 2001; Maier et al. 2002) but are still blocked by gap junction blockers (Hormuzdi et al. 2001), suggesting that VFOs depend on gap junctions not formed by Cx36.

Axonal gap junctions were first postulated to explain fast spikelets (on the order of a few milliseconds) seen in hippocampal pyramidal cell somata. These spikelets were confirmed to originate from axonal gap junctions through simulations (Draguhn et al. 1998) and experiment (Schmitz et al. 2001). Fast spikelets are seen in neocortical pyramidal cells as well (Cunningham et al. 2004; Steriade et al. 1993). These spikelets differ from spikelets originating from basal dendrites in that dendritic spikelets are not as prominent when triggered synaptically (Acker and Antic 2009; Milojkovic et al. 2005) and may have a slower time scale than when they originate from a gap junction (Gansert et al. 2007; Nadim and Golowasch 2006). The spikelets shown in Cunningham et al. (2004); Steriade et al. (1993) are also all-or-none events that are sensitive to the somatic voltage, which is in line with our results for axonal gap junctions.

Limitations of the Model

While the findings of our model are robust with respect to the parameters we considered, there are many other details that could be explored further. For instance, we used only standard Hodgkin-Huxley Na^+ and K^+ conductances, while axons may have many other currents (Debanne 2004; Shu et al. 2006, 2007b). We varied g_{Na} and g_K together, while g_K may affect excitability in its own right. While modest changes in the somatic leak conductance did not significantly change the results, larger changes may affect AP propagation more and could provide alternate boundaries for the window of control. We did not take myelination into account, which may affect AP propagation from a collateral into the main axon. There may also be other means of control that we are not currently aware of, such as neuromodulators, pH, and glial cells.

While our network model uses realistic parameters, it is still drastically simplified. For example, in the neocortex minicolumns do not form a perfectly regular hexagonal grid, and there is heterogeneity in the number of cells in a column. The network connections are largely random, and the distribution of gap junctions among cells is largely unknown.

Axons are very thin, which brings the accuracy of the diameters reported in the 3D cell reconstructions into question. We inquired of each laboratory whether diameter was taken into account in their reconstructions. We excluded those reconstructions that did not account for diameter from our analysis of AP propagation. Out of the reconstructions we used to analyze AP propagation, diameters reported were often below 1 μm with one or two significant digits. Therefore, diameters were probably rounded to the nearest digit or whole fraction of 1 μm. Since our results on AP propagation from axon collaterals rely on the heterogeneity of axon diameters, and diameter rounding would reduce the heterogeneity, we expect our results to hold if more accurate diameters are used.

There may be more overlap between windows of control for AP propagation from collaterals if other conductances are used. The windows of control produced with conductances from Schmidt-Hieber et al. (2008) overlapped slightly more than the ones produced with conductances from Traub et al. (2005a).

Summary

We have shown that pyramidal cell depolarization enables APs to cross gap junctions in the IS and main axon, while hyperpolarization blocks APs at IS and main axon gap junctions. While the somatic voltage may not effectively control AP propagation from all axon collaterals and across some IS and main axon gap junctions, the number of pyramidal cells hardwired together is limited. Therefore, neocortical pyramidal cells may send signals to postsynaptic cells simply by depolarizing. Groups of cells depolarized together may form cell assemblies, and large assemblies can supply tetanic stimulation to postsynaptic cells. Too many uncontrollable connections may lead to abundant uncontrolled VFOs, kindling postsynaptic cells which may lead to epilepsy. Although the modeled network has limitations, it presents plausible mechanisms for control within an axonal plexus, thus opening the possibility for richer methods of neural coding.

APPENDIX A: GAP JUNCTION CONDUCTANCES REPORTED IN EXPERIMENT

In our model, the window of control contains the IS default g_{Na} for gap junction conductances of 10–24 nS. Here, we relate these conductances to the results reported in Wang et al. (2010). In Wang et al. (2010), the subthreshold coupling coefficient (*CC*) has a mean and standard deviation of 54 $\pm$ 27%, with a range of 20%−93%. To compute coupling coefficients for our model, we set the somatic leak conductance to $g_L = 2 \times 10^{-5}$ S/cm^2. This yields an input resistance of 131 MΩ, which more accurately reflects the input resistance of cells recorded in Wang et al. (2010) since they were in quiescent slices.

Figure A1 shows the coupling coefficients computed with our model for a range of gap junction conductances. The mean coupling

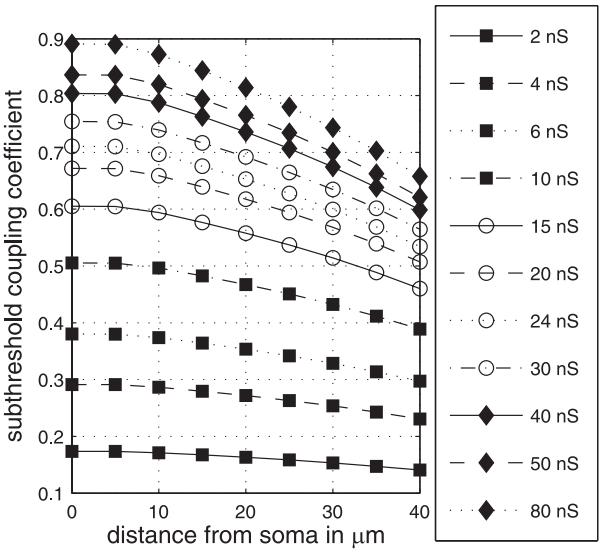

Fig. A1. Step coupling coefficient for gap junctions in the IS. Layer 5 simplified axon model. Somatic leak conductance is $g_L = 2 \times 10^{-5}$ S/cm^2 to match the input resistance of the cells in vitro in Wang et al. (2010). Step coupling coefficient for layer 5 pyramidal cells, as reported in Wang et al. (2010), is 54 ± 27% with a range of 20–93%. Indicated is that gap junction conductances of 2–80 nS in our model cover this range. Also shown is that the coupling coefficient recorded in the soma decreases as the gap junction moves away from the soma. From this, the mean coupling coefficient reported in Wang et al. (2010) corresponds to a gap junction at the soma with conductance of ~10 nS.

coefficient reported in Wang et al. (2010) corresponds to a gap junction at the soma with $g_{gj} \approx 10$ nS in our model, while one standard deviation above and below corresponds to $g_{gj} \approx 40$ and 4 nS, respectively. The coupling coefficient, as measured from the soma, decreases as the gap junction moves away from the soma. This means that low coupling coefficients reported in Wang et al. (2010) may correspond to gap junctions farther from the soma instead of gap junctions with $g_{gj} < 10$ nS at the soma. Therefore, these connections may be in the window of control at their location. However, high coupling coefficients reported in Wang et al. (2010) probably do reflect gap junctions close to the soma. Therefore high coupling coefficients may correspond to gap junctions with $g_{gj} > 24$ nS in our model and may not be controllable by the somatic voltage. Assuming that the coupling coefficients in Wang et al. (2010) follow a Gaussian distribution and that the somatic voltage can control AP propagation for gap junctions with $g_{gj} \leq 24$ nS or $CC \leq 70\%$ at the soma, the somatic voltage can control AP propagation across ≤70% of gap junctions in the IS.

APPENDIX B: DETAILED ANALYSIS OF N_{VFO}

Relative Amplitude of VFOs in the Field Potential

Figure 5 of Grenier et al. (2001) shows the relative amplitude of VFOs vs. the somatic voltage during the slow oscillation induced by ketamine-xylazine anesthesia in a cat. The relative amplitude is the amplitude divided by the maximum amplitude observed. The amplitude of VFOs is very small but is not zero when the somatic voltage is low. When there is a low level of VFOs, the VFO amplitude may be generated from cells actually firing at VFO frequencies, cells that have noisy membrane potentials, or a mixture of both. [There is little synaptic activity during the down state of the slow oscillation (Steriade et al. 2001; Timofeev et al. 2001).] To determine how many cells may be firing at VFO frequencies vs. noisy cells, we developed a formula for the relative amplitude of the field potential at a fixed frequency that can be compared directly to the data presented in Grenier et al. (2001; Fig. 5).

Suppose the field potential at time j (v_j) is composed of two time series:

$$v_j = w_j + X_j,$$

where w_j is deterministic and X_j is random with mean 0 and standard deviation σ. The amplitude of the time series $\{V_j\}_{j=0}^{N-1}$ at frequency $2\pi k$ is $\sqrt{E(|\hat{v}_k|^2)}$ where

$$E\left(|\hat{v}_k|^2\right) = |\hat{w}_k|^2 + \sigma^2$$

and $\hat{v}_k = \sum_{j=0}^{N-1} v_j e^{-2\pi ijk/N}$ is the discrete Fourier transform (Munro and Börgers 2010). Let M be the total number of cells that produce the field potential, m of which are firing at frequency $2\pi k$ while the rest have noisy membrane potentials. Let $v_{\ell,j} = w_{\ell,j} + X_{\ell,j}$ be the extracellular field potential next to the ℓth cell at time j. [See Murakami et al. (2002) for a quantitative assessment on how the membrane potential relates to the extracellular field potential.] The field potential at time j may be approximated by:

$$v_j = \frac{1}{M}\sum_{\ell=1}^{M} v_{\ell,j} = \frac{1}{M}\sum_{\ell=1}^{m} w_{\ell,j} + \frac{1}{M}\sum_{\ell=m+1}^{M} X_{\ell,j}$$

and so

$$E\left(|\hat{v}_k|^2\right) = \left|\frac{1}{M}\sum_{\ell=1}^{m}\hat{w}_{\ell,k}\right|^2 + var\left(\frac{1}{M}\sum_{\ell=m+1}^{M} X_{\ell,j}\right).$$

Assuming that the amplitudes of the oscillating cells ($|\hat{w}_{\ell,k}|$) are all the same:

$$\begin{aligned}\left|\frac{1}{M}\sum_{\ell=1}^{m}\hat{w}_{\ell,k}\right|^2 &= \frac{1}{M^2}\sum_{\ell_1=1}^{m}\hat{w}_{\ell_1,k}\sum_{\ell_2=1}^{m}\overline{\hat{w}_{\ell_2,k}} \\ &= \frac{1}{M^2}\sum_{\ell_1=1}^{m}\sum_{\ell_2=1}^{m}\hat{w}_{\ell_1,k}\overline{\hat{w}_{\ell_2,k}} \\ &= \frac{1}{M^2}\sum_{\ell_1=1}^{m}\sum_{\ell_2=1}^{m}|\hat{w}_{\ell_1,k}|^2 \\ &= \frac{1}{M^2}\sum_{\ell=1}^{m} m|\hat{w}_{\ell,k}|^2 \\ &= \frac{m^2}{M^2}|\hat{w}_{\ell,k}|^2\end{aligned}$$

Likewise, assuming that all noisy cells have the same variance (σ_ℓ):

$$\begin{aligned}var\left(\frac{1}{M}\sum_{\ell=m+1}^{M} X_{\ell,j}\right) &= \frac{1}{M^2}\sum_{\ell=m+1}^{M} var\left(X_{\ell,j}\right) \\ &= \frac{1}{M^2}\sum_{\ell=m+1}^{M}\sigma_\ell^2 = \frac{M-m}{M^2}\sigma_\ell^2.\end{aligned}$$

Thus the expected amplitude at frequency $2\pi k$ is:

$$\sqrt{E\left(|\hat{v}_k|^2\right)} = \sqrt{\frac{m^2}{M^2}|\hat{w}_{\ell,k}|^2 + \frac{M-m}{M^2}\sigma_\ell^2}.$$

Suppose there are m_{max} cells firing at frequency $2\pi k$ when the maximum VFO amplitude is observed and $\sigma_\ell = \alpha|\hat{w}_{\ell,k}|$, then the relative amplitude is:

$$RA = \frac{\sqrt{\frac{m^2}{M^2}|\hat{w}_{\ell,k}|^2 + \frac{M-m}{M^2}\sigma_\ell^2}}{\sqrt{\frac{m_{max}^2}{M^2}|\hat{w}_{\ell,k}|^2 + \frac{M-m_{max}}{M^2}\sigma_\ell^2}} = \frac{\sqrt{m^2 + \alpha^2(M-m)}}{\sqrt{m_{max}^2 + \alpha^2(M-m_{max})}} \quad (B1)$$

We can then interpret a relative amplitude at "noise level" to be the value of RA when $m = 0$.

Estimate of N_{VFO} Based on RA

Our results show that cell hyperpolarization blocks gap junctions between IS and main axons. This means that RA should decrease with the somatic voltage until all controllable gap junctions are blocked when V_s reaches a threshold voltage V_{min}. Once the somatic voltage of all cells falls below V_{min}, the relative amplitude of VFOs will reach a minimum, RA_{min}. The higher RA_{min} is, the higher the possible number of cells participating in a VFO when cells are hyperpolarized. In Grenier et al. (2001; Fig. 5), it appears that RA_{min} can be as high as approximately 0.01, which is the amplitude corresponding to V_{min} approximately equal to −83.

To estimate m_{min}, the number of cells firing at VFO frequencies when $RA = RA_{min}$, we first solve *Eq. B1* for m:

$$m = \frac{\alpha^2 + \sqrt{\alpha^4 - 4\left(\alpha^2 M - RA^2\left(m_{max}^2 + \alpha^2\left(M - m_{max}\right)\right)\right)}}{2}$$

and estimate M and m_{max}. We first estimate M. The depth electrodes in Grenier et al. (2001) were placed 0.8–1 mm underneath the pial surface, which may correspond to layer 5 according to Skoglund et al. (1996). While the depth electrodes were placed 1.5 mm apart in Grenier et al. (2001), their range is uncertain. However, activity generating the local field potential should be within 1 mm^2 (Katzner et al. 2009). Therefore, we estimate that M ranges from the number of cells in layer 5 underneath 1 mm^2 of cortex (23,000; Skoglund et al. 1996) to all cells underneath 1 mm^2 or cortex (133,000; Skoglund et al. 1996). We now estimate the range of m_{max}. Since ~85% of cells in the rat somatosensory cortex are pyramidal cells (Beaulieu 1993), there are $\sim 0.85 \times 23{,}000 = 19{,}550$ pyramidal cells in layer 5 under 1 mm^2 of cortical surface. Assuming that pyramidal cells electrically couple only to cells in the same layer (Gutnick et al. 1985), this means that there can be up to 19,500 cells participating in an axonal plexus. At least 30% of pyramidal cells may contribute to the maximum VFO amplitude, since Steriade et al. (1993) found that 30% of pyramidal cells display spikelets during slow oscillations. At the same time, at most 2/3 of pyramidal cells are likely to contribute to the maximum amplitude, since ~2/3 of cells participated in a VFO for the model in Traub et al. (1999) where the rate of connectivity may have been overestimated (Gutnick et al. 1985). Thus we estimate m_{max} to range from (0.3)19,550 to (2/3)19,550. Figure B1 shows values for m_{min} with these values of M and m_{max}, $RA = RA_{min}$, and α ranging from 0 to 1. Over all of these parameters, m_{min} can range from 0 to 130 cells.

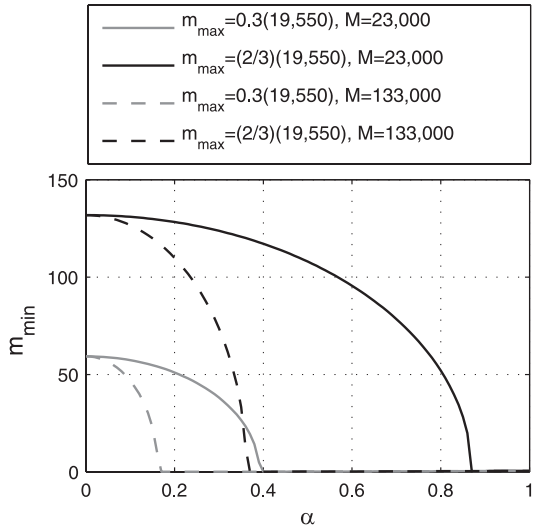

Fig. B1. Estimates for m_{min} show that the maximum number of cells that may participate in a VFO when cells are hyperpolarized is ~130. These values for m_{min} are calculated assuming that M and m_{max} are at the extremes of their estimated range. Largest values of m_{min} occur for higher values of m_{max} when $\alpha = 0$.

Therefore, our bound on the number of cells participating in a VFO during cell hyperpolarization is $N_{\mathrm{VFO}} \approx 130$.

APPENDIX C: PROBABILITY OF FORMING CYCLES DECREASES WITH N_{CC} AND p_{INTRA}

Probability of Two Axons Connecting

Here, we derive the probability of two axons forming a gap junction on their collaterals based on the total length of each axon. If there are two axons in a slab of cortical tissue, one that is L_i μm long and one that is L_j μm long, what is the probability that they are connected by a gap junction? Consider each axon broken into r_i and r_j sections, respectively, with length ℓ each. We model p_ℓ, the probability that two sections (one from each axon) are connected as:

$$p_\ell \approx p\ell^2$$

given $0 < \ell \ll 1$ and p is the probability that 2-μm sections of axon will find each other in the cortical slab and form a gap junction. The probability that none of the sections are connected is

$$\left(1 - p_\ell\right)^{r_i r_j} = \left(1 - p_\ell\right)^{\frac{L_i L_j}{\ell^2}}.$$

Taking the limit as $\ell \to 0$, we obtain:

$$\lim_{\ell\to 0}\left(1 - p_\ell\right)^{\frac{L_i L_j}{\ell^2}} \approx \lim_{\ell\to 0}\left(1 - p\ell^2\right)^{\frac{L_i L_j}{\ell^2}} = \alpha$$

$$\ln(\alpha) = \lim_{\ell\to 0}\frac{L_i L_j}{\ell^2}\ln\left(1 - p\ell^2\right)$$

$$= \lim_{\ell\to 0}\frac{\ln\left(1 - p\ell^2\right)}{\frac{\ell^2}{L_i L_j}}$$

$$= \lim_{\ell\to 0}\frac{\frac{-2p\ell}{\left(1 - p\ell^2\right)}}{\frac{2\ell}{L_i L_j}}$$

$$= \lim_{\ell\to 0}\frac{-pL_i L_j}{1 - p\ell^2}$$

$$= -pL_i L_j$$

$$\alpha = e^{-pL_i L_j}.$$

Therefore the probability that there is at least one connection between axons i and j is

$$p_{i,j} = 1 - e^{-pL_i L_j} = f(p).$$

If we Taylor expand $p_{i,j} = f(p)$ about 0, then

$$p_{i,j} = f(0) + f'(0)p + \frac{f''(0)}{2}p^2 + \cdots$$

$$= 1 - 1 + L_i L_i p - \frac{\left(L_i L_j\right)^2}{2}p^2 + \cdots$$

$$\approx L_i L_i p$$

if $p \ll 1/(L_i L_j)$.

Estimating d, the Average Degree of a Cell

To estimate d, the expected average degree (or number of connections) of a cell, we first focus on the expected degree of one particular cell. Suppose that cell 0 has length L_0. Cells can form an IS/MA gap junctions connection with probability p_{intra} to any other cell within the

same column. Cells can form a collateral gap junction connection to any other cell within r_c units on the hexagonal grid. Let M be the total number of potential neighbors within reach of cell 0. Suppose that each potential neighbor has a different length: $L_1, L_2, \ldots, L_M$. If we can take the approximation $p_{i,j} \approx pL_iL_j$, then the expected average degree of cell 0 (d_0) is:

$$\begin{aligned} d_0 &\approx p_{intra}(n_{cc} - 1) + pL_0L_1 + pL_0L_2 + \cdots + pL_0L_M \\ &= p_{intra}(n_{cc} - 1) + pL_0\sum_{k=1}^{M} L_k. \end{aligned}$$

Therefore, an approximation for d is:

$$\begin{aligned} d &= E(d_0) \\ &\approx p_{intra}(n_{cc} - 1) + pE(L_0)\sum_{k=1}^{M} E(L_k) \\ &= p_{intra}(n_{cc} - 1) + pL\sum_{k=1}^{M} L \\ &= p_{intra}(n_{cc} - 1) + pL(ML) \\ &= p_{intra}(n_{cc} - 1) + pL^2M. \end{aligned}$$

The estimates $d \approx [p_{intra}(n_{cc} - 1) + pL^2M]$ and $p_{i,j} \approx pL_iL_j$ are reasonable if $p \ll 1/(L_iL_j)$ or $pL_iL_j \ll 1$. If we set

$$p = (d_w - p_{intra}(n_{cc} - 1))/(L^2M) \qquad (C1)$$

where d_w is the desired expected degree, then what is the maximum value for pL_iL_j? The number of cells per column can range from 3 to 20 cells (Mountcastle 1997; Rockland and Ichinohe 2004). A simple calculation shows that $M = 3r_c(r_c + 1)n_{cc} + n_{cc} - 1$. This means that M can range from 812 to 5,419 cells. The maximum value of pL_iL_j over all values of p, L_i, L_j, and M is 0.0065 when $d_w = 1$. Since we are interested in finding cycles when there is no large cluster, we choose $d_w \leq 1$ (Chung and Lu 2002). Therefore, if we set p according to *Eq. C1* above, then $d \approx [p_{intra}(n_{cc} - 1) + pL^2M] = d_w$ is a reasonable estimate for the expected average degree. We use this estimate as the expected average degree for the rest of our calculations.

Finding a Cycle Through a Branching Process

Here, we justify the assumption that the probability of forming a cycle is minimized when $n_{cc} = 20$ and $p_{intra} = 0$, given that clusters are the same size. First, we derive a formula for $g(n_{cc}, p_{intra})$, which represents the probability of forming a cycle in terms of n_{cc} and p_{intra} assuming a given fixed average degree d. We derive $g(n_{cc}, p_{intra})$ under one assumption. Let C be a cell in a cluster whose connections we are determining. Let β be the ratio of cells in the cluster within r_c of C out of the total number of cells in the cluster. We assume that β is constant as M increases (see Fig. C1). Then we show that $g(n_{cc}, p_{intra})$ is minimized when $n_{cc} = 20$ and $p_{intra} = 0$. Finally, we confirm that cluster sizes are maximized when $p_{intra} = 0$ and $n_{cc} = 20$. Thus, as (n_{cc}, p_{intra}) approaches (20, 0), the probability of forming a cycle decreases while cluster sizes increase.

We first fix d by setting

$$p = (d_w - p_{intra}(n_{cc} - 1))/(L^2M).$$

with d fixed, the probability that two cells, i and j, will connect if they are in different columns as a function of n_{cc} is

$$\begin{aligned} p_{i,j} &= 1 - e^{-pL_iL_j} \\ &= 1 - exp\left(-\frac{d - p_{intra}(n_{cc} - 1)}{L^2M}L_iL_j\right) = 1 - exp\left(-\frac{d - p_{intra}(n_{cc} - 1)}{M}\frac{L_iL_j}{L^2}\right) \end{aligned}$$

where L_i is the length of cell i and L_j is the length of cell j. The probability that cells i and j will connect if they are in the same column is

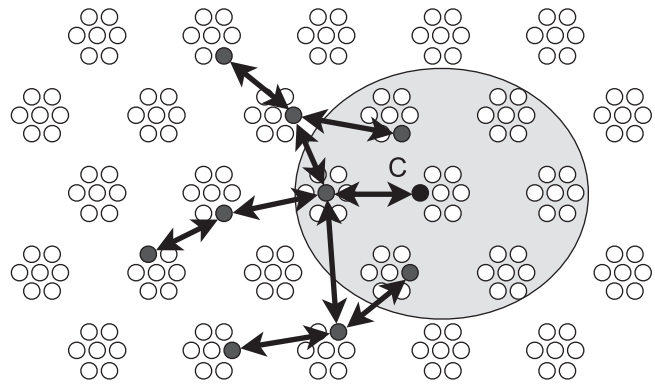

Fig. C1. Assumption on β, the ratio of cells in the cluster within r_c of a single *cell C* the connections of which are being determined, out the total number of cells already in the cluster. *Cell C* is labeled in black, while other cells in the cluster are filled in gray. Shaded region encloses the cells within $r_c = 1$ units on the hexagonal grid of C. As n_{cc} increases, the expected degree of cells in the cluster and the size of the cluster increases in a spatially uniform manner. Therefore, it is reasonable to assume that the proportion of cells in the cluster inside the shaded region relative to outside should remain the same. Hence, β is constant with respect to n_{cc}.

$$p_{i,j} = 1 - (1 - p_{intra})(e^{-pL_iL_j}).$$

We form a cluster in the network by first choosing a random cell A. For each of A's possible neighbors, j, we connect cells A and j with probability $p_{A,j}$. Then, we determine the connections for every neighbor of A, B, by connecting possible neighbors of B, k, with probability $p_{B,k}$. We repeat the process for neighbors two steps away from A (A's neighbors' neighbors), three steps away from A, and so on. Meanwhile, we keep a list of all the cells connected to A through this cluster. We continue this process until *1*) we connect a cell to potential neighbor that is already listed, or *2*) there are no more new cells to connect. If we connect a cell to potential neighbor that is already listed, then we form a cycle.

In determining the connections of any cell C (with the exception of the first cell A), there is a chance that we may connect cell C to a cell that is already listed. Suppose Y cells are already listed and that βY of those cells are potential neighbors of C. Then the probability that cell C with length L_C will connect to one of the cells already listed is:

$$\begin{aligned} g(n_{cc}, p_{intra}) &= 1 - \prod_{j=1}^{\beta Y}(1 - p_{C,j}) \\ &= 1 - \prod_{j=1}^{n_{cc}-1}(1 - p_{C,j})\prod_{j=n_{cc}}^{\beta Y}(1 - p_{C,j}) \\ &= 1 - \prod_{j=1}^{n_{cc}-1}(1 - p_{intra})e^{-pL_CL_j}\prod_{j=n_{cc}}^{\beta Y}e^{-pL_CL_j} \\ &= 1 - (1 - p_{intra})^{(n_{cc}-1)}\prod_{j=1}^{\beta Y}e^{-pL_CL_j} \\ &= 1 - (1 - p_{intra})^{(n_{cc}-1)}e^{\sum_{j=1}^{\beta Y} -pL_CL_j} \\ &= 1 - \exp\left[(n_{cc} - 1)\ln(1 - p_{intra}) - pL_C\sum_{j=1}^{\beta Y}L_j\right] \end{aligned}$$

The length of cell C, L_C, is fixed with respect to n_{cc}. By assumption, β does not change with n_{cc} either (see Fig. C1). However, the lengths of cells already on the list (L_j) and the total number of cells on the list (Y) may change with n_{cc} and p_{intra}. To address this, we calculate the expected length of a listed cell $E[L_j \mid \text{cell } j \text{ is listed}]$ and the expected length of the list $E[Y]$ as a function of n_{cc} and p_{intra}.

To calculate $E[L_j \mid \text{cell } j \text{ is listed}]$, let T be the total number of cell lengths to choose from. Then:

$$
\begin{aligned}
&P\big(L_j=\ell_j|\text{ cell } j \text{ is listed}\big)\\
&=\frac{P\big(L_j=\ell_j \text{and cell } j \text{is listed}\big)}{P\big(\text{cell } j \text{ is listed}\big)}\\
&=\frac{P\big(\text{cell } j \text{is listed} \mid L_j=\ell_j\big)P\big(L_j=\ell_j\big)}{\sum_{k=1}^{T}P\big(\text{cell } j \text{is listed} \mid L_j=\ell_k\big)P\big(L_j=\ell_k\big)}\\
&=\frac{\big(1-e^{-pL_C\ell_j}\big)\left(\frac{1}{T}\right)}{\sum_{k=1}^{T}\big(1-e^{-pL_C\ell_k}\big)\left(\frac{1}{T}\right)}\\
&=\frac{\big(1-e^{-pL_C\ell_j}\big)}{\sum_{k=1}^{T}\big(1-e^{-pL_C\ell_k}\big)}
\end{aligned}
$$

and

$$
\begin{aligned}
E\big[L_j|\text{ cell } j \text{ is listed}\big]&=\sum_{i=1}^{T}\ell_i P\big(L_j=\ell_i|\text{cell } j \text{is listed}\big)\\
&=\sum_{i=1}^{T}\frac{\ell_i\big(1-e^{-pL_C\ell_j}\big)}{\sum_{k=1}^{T}\big(1-e^{-pL_C\ell_k}\big)}\\
&=\frac{\sum_{i=1}^{T}\ell_i\big(1-e^{-pL_C\ell_i}\big)}{\sum_{k=1}^{T}\big(1-e^{-pL_C\ell_k}\big)}
\end{aligned}
$$

To calculate $E[Y]$, we first calculate the expected degree of a random cell as a function of n_{cc} and p_{intra}. The expected degree of a random cell 0 with length L_0 is:

$$
\begin{aligned}
d_0&\approx p_{intra}\big(n_{cc}-1\big)+pL_0\sum_{k=1}^{M}L_k\\
&=p_{intra}\big(n_{cc}-1\big)+\frac{d-p_{intra}\big(n_{cc}-1\big)}{L^2M}L_0\sum_{k=1}^{M}L_k\\
&=p_{intra}\big(n_{cc}-1\big)+\frac{d-p_{intra}\big(n_{cc}-1\big)}{L^2}L_0\frac{1}{M}\sum_{k=1}^{M}L_k\\
&\approx p_{intra}\big(n_{cc}-1\big)+\frac{d-p_{intra}\big(n_{cc}-1\big)}{L}L_0.
\end{aligned}
$$

Therefore, the expected degree of a cell that is already listed is:

$$
\begin{aligned}
E\big[\text{degree of listed cell}\big]&=E\big[d_0 \mid \text{cell 0 is listed}\big]\\
&\approx p_{intra}\big(n_{cc}-1\big)\\
&\quad+\frac{d-p_{intra}\big(n_{cc}-1\big)}{L}E\big[L_j \mid \text{cell } j \text{ is listed}\big].
\end{aligned}
$$

According to Newman (2003), the average number of neighbors m steps away from A is:

$$
\begin{aligned}
z_m&=\left[\frac{E\big[\text{degree of listed cell}\big]}{E\big[\text{degree of any cell}\big]}\right]^{m-1}E\big[\text{degree of any cell}\big]\\
&=\left[\frac{E\big[\text{degree of listed cell}\big]}{d}\right]^{m-1}d\\
&=z^{m-1}d
\end{aligned}
$$

Thus the expected number of cells on the list when we are n steps away from A is:

$$
\begin{aligned}
E\big[Y\big]&=1+\sum_{m=1}^{n}z_m\\
&=1+\sum_{m=1}^{n}z^{m-1}d\\
&=1+\sum_{m=1}^{n-1}z^{m}d\\
&=1+d\frac{1-z^n}{1-z}
\end{aligned}
\qquad (C2)
$$

Substituting $E[L_j|\text{cell } j \text{ is listed}]$ for L_j and $E[Y]$ for Y in *Eq. C3*, we have:

$$
\begin{aligned}
g\big(n_{cc},p_{intra}\big)&\approx 1-\exp\Bigg[\big(n_{cc}-1\big)\ln\big(1-p_{intra}\big)\\
&\quad-\left(\frac{d-p_{intra}\big(n_{cc}-1\big)}{L^2M}\right)L_C\sum_{j=1}^{\beta E[Y]}E\big[L_j \mid \text{cell } j \text{is listed}\big]\Bigg]\\
&=1-\exp\Bigg[\big(n_{cc}-1\big)\ln\big(1-p_{intra}\big)\\
&\quad-\left(\frac{d-p_{intra}\big(n_{cc}-1\big)}{L^2M}\right)L_C\beta E\big[Y\big]E\big[L_j \mid \text{cell } j \text{is listed}\big]\Bigg]
\end{aligned}
$$

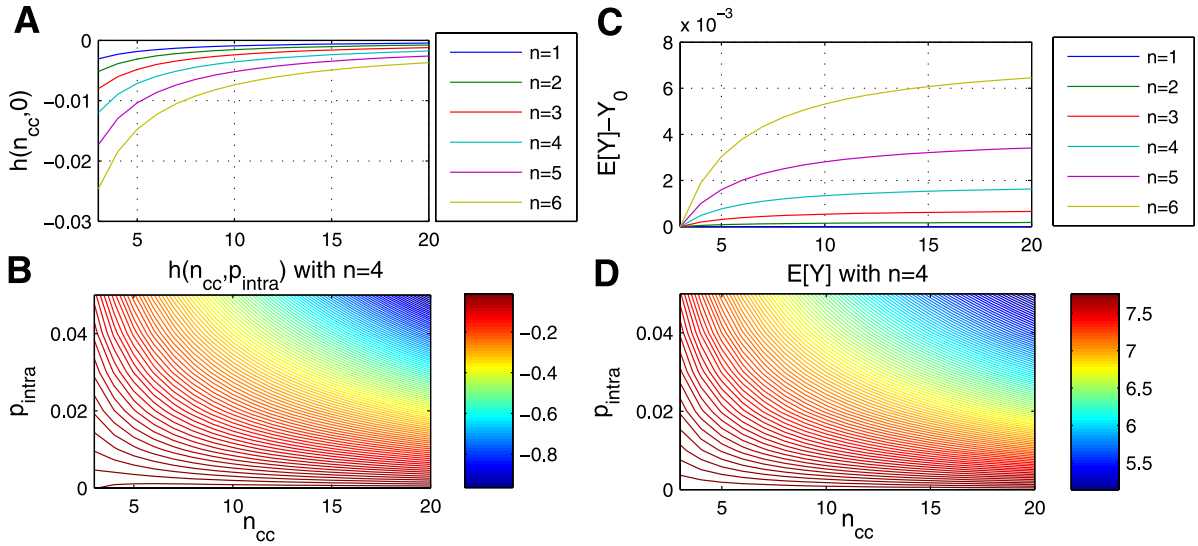

Fig. C2. $h(n_{cc}, p_{intra})$ and $E[Y]$ are maximized when $n_{cc} = 20$ and $p_{intra} = 0$. Calculations are made with weights from the layer 5 cell reconstructions, $d = 1$, $\beta = 1$, and L_0 is chosen randomly ($L_0 \approx 104$). n stands for the number of steps cell C is away from cell A in the branching process. *A*: $h(n_{cc}, p_{intra})$ increases with n_{cc} when $p_{intra} = 0$. *B*: $h(n_{cc}, p_{intra})$ increases as p_{intra} decreases. *A* and *B* imply that the maximum $h(n_{cc}, p_{intra})$ is reached when $n_{cc} = 20$ and $p_{intra} = 0$. *C*: $E[Y] - Y_0$ when $p_{intra} = 0$, where Y_0 is the value of $E[Y]$ when $n_{cc} = 3$. We can see that $E[Y]$ marginally increases with n_{cc} when $p_{intra} = 0$. D: $E[Y]$ increases as p_{intra} decreases. This implies that cluster sizes are maximized when $n_{cc} = 20$ and $p_{intra} = 0$.

$$= 1 - \exp\left[h(n_{cc}, p_{intra})\right]$$

Figure C2 shows that the function $h(n_{cc}, p_{intra})$ in maximized when n_{cc} is high and $p_{intra} = 0$. Since $g(n_{cc}, p_{intra})$ is minimized when $h(n_{cc}, p_{intra})$ is maximized, the probability of connections from cell C forming a cycle are minimized when $n_{cc} = 20$ and $p_{intra} = 0$ when d is fixed. Figure 17 also shows that $E[Y]$ is also maximized when $n_{cc} = 20$ and $p_{intra} = 0$. This means that cluster sizes for fixed d are maximized when $n_{cc} = 20$ and $p_{intra} = 0$. Therefore, the number of cells required in a cluster to form a cycle is maximized when $n_{cc} = 20$ and $p_{intra} = 0$.

ACKNOWLEDGMENTS

We acknowledge Roger Traub for help with some of the modeling decisions made in this paper. We thank Yun Wang for discussing results in Wang et al. (2010), which inspired the network model, and Steve Epstein who helped in editing the paper. We also thank neuromorpho.org and the authors who contributed reconstructions, without which this work would not have been possible.

GRANTS

E. Munro was funded by an National Science Foundation (NSF) Mathematical Sciences Postdoctoral Research Fellowship, NSF Award Number 0802889, NSF DMS-0602204 "Enhancing the Mathematical Sciences Workforce in the 21st Century (EMSW21): Biodynamics at Boston University", and the RIKEN Brain Science Institute (Wako-shi, Japan). N. Kopell was funded by NSF DMS-0717670 "Mathematical Analysis of Neural Dynamics with Multiple Frequencies."

DISCLOSURES

No conflicts of interest, financial or otherwise, are declared by the author(s).

REFERENCES

Acker CD, Antic SD. Quantitative assessment of the distributions of membrane conductances involved in action potential backpropagation along basal dendrites. *J Neurophysiol* 101: 1524–1541, 2009.

Ascoli GA, Donohue DE, Halavi NeuroMorpho M. Org: A central resource for neuronal morphologies. *J Neurosci* 27: 9247–9251, 2007.

Beaulieu C. Numerical data on neocortical neurons in adult rat, with special reference to the GABA population. *Brain Res* 609: 284–292, 1993.

Bertram E. The relevance of kindling for human epilepsy. *Epilepsia* 48, *Suppl* 2: 65–74, 2007.

Boiko T, Wart AV, Caldwell JH, Levinson SR, Trimmer JS, Matthews G. Functional specialization of the axon initial segment by isoform-specific sodium channel targeting. *J Neurosci* 23: 2306–2313, 2003.

Bragin A, Mody I, Wilson CL, Engel J Jr. Local generation of fast ripples in epileptic brain. *J Neurosci* 22: 2012–2021, 2002.

Bragin A, Wilson CL, Almajano J, Mody I, Engel J Jr. High-frequency oscillations after status epilepticus: epileptogenesis and seizure genesis. *Epilepsia* 45: 1017–1023, 2004.

Brecht M, Sakmann B. Dynamic representation of whisker deflection by synaptic potentials in spiny stellate and pyramidal cells in the barrels and septa of layer 4 rat somatosensory cortex. *J Physiol* 543: 49–70, 2002.

Brosch M, Budinger E, Scheich H. Stimulus-related gamma oscillations in primate auditory cortex. *J Neurophysiol* 87: 2715–2725, 2002.

Brovelli A, Lachaux JP, Kahane P, Boussaoud D. High gamma frequency oscillatory activity dissociates attention from intention in the human premotor cortex. *Neuroimage* 28: 154–164, 2005.

Buhl DL, Harris KD, Hormuzdi SG, Monyer H, Buzsáki G. Selective impairment of hippocampal gamma oscillations in connexin-36 knock-out mouse in vivo. *J Neurosci* 23: 1013–1018, 2003.

Buxhoeveden DP, Casanova MF. The minicolumn hypothesis in neuroscience. *Brain* 125: 935–951, 2002.

Canolty RT, Soltani M, Dalal SS, Edwards E, Dronkers NF, Nagarajan SS, Kirsch HE, Barbaro NM, Knight RT. Spatiotemporal dynamics of word processing in the human brain. *Front Neurosci* 1: 185–196, 2007.

Carnevale NT, Hines ML. *The NEURON Book*. Cambridge, UK: Cambridge University Press, 2006.

Chang BS, Lowenstein DH. Epilepsy. *N Engl J Med* 349: 1257–1266, 2003.

Chevassus-au-Louis N, Baraban SC, Gäıarsa JL, Ben-Ari Y. Cortical malformations and epilepsy: new insights from animal models. *Epilepsia* 40: 811–821, 1999.

Cheyne D, Bells S, Ferrari P, Gaetz W, Bostan AC. Self-paced movements induce high-frequency gamma oscillations in primary motor cortex. *Neuroimage* 42: 332–342, 2008.

Chung F, Lu L. Connected components in random graphs with given expected degree sequences. *Ann Comb* 6: 125–145, 2002.

Cox CL, Denk W, Tank DW, Svoboda K. Action potentials reliably invade axonal arbors of rat neocortical neurons. *Proc Natl Acad Sci USA* 97: 9724–9728, 2000.

Crochet S, Petersen CCH. Correlating whisker behavior with membrane potential in barrel cortex of awake mice. *Nat Neurosci* 9: 608–610, 2006.

Crone NE, Sinai A, Korzeniewska A. High-frequency gamma oscillations and human brain mapping with electrocorticography. *Prog Brain Res* 159: 275–295, 2006.

Cunningham MO, Halliday DM, Davies CH, Traub RD, Buhl EH, Whittington MA. Coexistence of gamma and high-frequency oscillations in rat medial entorhinal cortex in vitro. *J Physiol* 559: 347–353, 2004.

Cvapp. *Cvapp* (Online). http://www.compneuro.org/CDROM/docs/cvapp.html.

Debanne D. Information processing in the axon. *Nat Rev Neurosci* 5: 304–316, 2004.

Debanne D, Gúerineau NC, Gähwiler BH, Thompson SM. Action-potential propagation gated by an axonal I(A)-like K^+ conductance in hippocampus. *Nature* 389: 286–289, 1997.

Draguhn A, Traub RD, Schmitz D, Jefferys JG. Electrical coupling underlies high-frequency oscillations in the hippocampus in vitro. *Nature* 394: 189–192, 1998.

Edwards E, Soltani M, Deouell LY, Berger MS, Knight RT. High gamma activity in response to deviant auditory stimuli recorded directly from human cortex. *J Neurophysiol* 94: 4269–4280, 2005.

Edwards E, Soltani M, Kim W, Dalal SS, Nagarajan SS, Berger MS, Knight RT. Comparison of timefrequency responses and the event-related potential to auditory speech stimuli in human cortex. *J Neurophysiol* 102: 377–386, 2009.

Engel J Jr. Introduction to temporal lobe epilepsy. *Epilepsy Res* 26: 141–150, 1996.

Engel J Jr, Bragin A, Staba R, Mody I. High-frequency oscillations: what is normal and what is not? *Epilepsia* 50: 598–604, 2009.

Erdos P, Rényi A. On the evolution of random graphs. *Publ Math Inst Hung Acad Sci* 5: 17–61, 1960.

Feldman ML, Peters A. A study of barrels and pyramidal dendritic clusters in the cerebral cortex. *Brain Res* 77: 55–76, 1974.

Gansert J, Golowasch J, Nadim F. Sustained rhythmic activity in gap-junctionally coupled networks of model neurons depends on the diameter of coupled dendrites. *J Neurophysiol* 98: 3450–3460, 2007.

Gaona CM, Sharma M, Freudenburg ZV, Breshears JD, Bundy DT, Roland J, Barbour DL, Schalk G, Leuthardt EC. Nonuniform high-gamma (60–500 Hz) power changes dissociate cognitive task and anatomy in human cortex. *J Neurosci* 31: 2091–2100, 2011.

Goldstein SS, Rall W. Changes of action potential shape and velocity for changing core conductor geometry. *Biophys J* 14: 731–757, 1974.

Goodenough DA, Paul DL. Gap junctions. *Cold Spring Harb Perspect Biol* 1: a002576, 2009.

Grenier F, Timofeev I, Steriade M. Focal synchronization of ripples (80–200 Hz) in neocortex and their neuronal correlates. *J Neurophysiol* 86: 1884–1898, 2001.

Grenier F, Timofeev I, Steriade M. Neocortical very fast oscillations (ripples, 80–200 Hz) during seizures: intracellular correlates. *J Neurophysiol* 89: 841–852, 2003.

Gutnick MJ, Lobel-Yaakov R, Rimon G. Incidence of neuronal dye-coupling in neocortical slices depends on the plane of section. *Neuroscience* 15: 659–666, 1985.

Gutnick MJ, Prince DA. Dye coupling and possible electrotonic coupling in the guinea pig neocortical slice. *Science* 211: 67–70, 1981.

Hamzei-Sichani F, Kamasawa N, Janssen WGM, Yasumura T, Davidson KGV, Hof PR, Wearne SL, Stewart MG, Young SR, Whittington MA, Rash JE, Traub RD. Gap junctions on hippocampal mossy fiber axons demonstrated by thin-section electron microscopy and freeze fracture replica immunogold labeling. *Proc Natl Acad Sci USA* 104: 12548–12553, 2007.

Hines ML, Morse T, Migliore M, Carenvale NT, Shepherd GM. ModelDB: A database to support computational neuroscience. *J Comput Neurosci* 17: 7–11, 2004.

Hormuzdi SG, Pais I, LeBeau FE, Towers SK, Rozov A, Buhl EH, Whittington MA, Monyer H. Impaired electrical signaling disrupts gamma frequency oscillations in connexin 36-deficient mice. *Neuron* 31: 487–495, 2001.

Hromádka T, Zador A. Representations in auditory cortex. *Curr Opin Neurobiol* 19: 430–433, 2009.

Jacobs J, Kahana MJ. Neural representations of individual stimuli in humans revealed by gamma-band electrocorticographic activity. *J Neurosci* 29: 10203–10214, 2009.

Jones MS, Barth DS. Spatiotemporal organization of fast (>200 Hz) electrical oscillations in rat vibrissa/barrel cortex. *J Neurophysiol* 82: 1599–1609, 1999.

Jones MS, MacDonald KD, Choi B, Dudek FE, Barth DS. Intracellular correlates of fast (>200 Hz) electrical oscillations in rat somatosensory cortex. *J Neurophysiol* 84: 1505–1518, 2000.

Katzner S, Nauhaus I, Benucci A, Bonin V, Ringach DL, Carandini M. Local origin of field potentials in visual cortex. *Neuron* 61: 35–41, 2009.

Koester HJ, Sakmann B. Calcium dynamics associated with action potentials in single nerve terminals of pyramidal cells in layer 2/3 of the young rat neocortex. *J Physiol* 529: 625–646, 2000.

Kole MHP, Ilschner SU, Kampa BM, Williams SR, Ruben PC, Stuart GJ. Action potential generation requires a high sodium channel density in the axon initial segment. *Nat Neurosci* 11: 178–186, 2008.

Lewis TJ, Rinzel J. Self-organized synchronous oscillations in a network of excitable cells coupled by gap junctions. *Network* 11: 299–320, 2000.

Lewis TJ, Rinzel J. Topological target patterns and population oscillations in a network with random gap junctional coupling. *Neurocomputing* 38–40: 763–768, 2001.

Lorincz A, Nusser Z. Cell-type-dependent molecular composition of the axon initial segment. *J Neurosci* 28: 14329–14340, 2008.

Maier N, Güldenagel M, Söhl G, Siegmund H, Willecke K, Draguhn A. Reduction of high-frequency network oscillations (ripples) and pathological network discharges in hippocampal slices from connexin 36-deficient mice. *J Physiol* 541: 521–528, 2002.

Margrie TW, Brecht M, Sakmann B. In vivo, low-resistance, whole-cell recordings from neurons in the anaesthetized and awake mammalian brain. *Pflügers Arch* 444: 491–498, 2002.

MathWorks. *MATLAB* (Online). http://www.mathworks.com/products/matlab/.

Mercer A, Bannister AP, Thomson AM. Electrical coupling between pyramidal cells in adult cortical regions. *Brain Cell Biol* 35: 13–27, 2006.

Milojkovic BA, Wuskell JP, Loew LM, Antic SD. Initiation of sodium spikelets in basal dendrites of neocortical pyramidal neurons. *J Membr Biol* 208: 155–169, 2005.

Mountcastle VB. The columnar organization of the neocortex. *Brain* 120: 701–722, 1997.

Mountcastle VB. Introduction: computation in cortical columns. *Cereb Cortex* 13: 2–4, 2003.

Munro E, Börgers C. Mechanisms of very fast oscillations in networks of axons coupled by gap junctions. *J Comput Neurosci* 28: 539–555, 2010.

Murakami S, Zhang T, Hirose A, Okada YC. Physiological origins of evoked magnetic fields and extracellular field potentials produced by guinea-pig CA3 hippocampal slices. *J Physiol* 544: 237–251, 2002.

Nadim F, Golowasch J. Signal transmission between gap-junctionally coupled passive cables is most effective at an optimal diameter. *J Neurophysiol* 95: 3831–3843, 2006.

NeuroMorphoOrg. http://NeuroMorpho.org.

NEURON. http://www.neuron.yale.edu/neuron/.

Newman ME. Random graphs as models of networks. In: *Handbook of Graphs and Networks: From the Genome to the Internet*, edited by Bornholdt S, Schuster HG. Weinheim, Germany: Wiley-VCH Verlag, chapt 2, pp. 35–68. 2003.

Nimmrich V, Maier N, Schmitz D, Draguhn A. Induced sharp wave-ripple complexes in the absence of synaptic inhibition in mouse hippocampal slices. *J Physiol* 563: 663–670, 2005.

Palmer LM, Stuart GJ. Site of action potential initiation in layer 5 pyramidal neurons. *J Neurosci* 26: 1854–1863, 2006.

Parker PRL, Cruikshank SJ, Connors BW. Stability of electrical coupling despite massive developmental changes of intrinsic neuronal physiology. *J Neurosci* 29: 9761–970, 2009.

Pei X, Leuthardt EC, Gaona CM, Brunner P, Wolpaw JR, Schalk G. Spatiotemporal dynamics of electrocorticographic high gamma activity during overt and covert word repetition. *Neuroimage* 54: 2960–2972, 2011.

Pitkänen A, McIntosh TK. Animal models of post-traumatic epilepsy. *J Neurotrauma* 23: 241–261, 2006.

Rakic P. Confusing cortical columns. *Proc Natl Acad Sci USA* 105: 12099–12100, 2008.

Rockland KS, Ichinohe N. Some thoughts on cortical minicolumns. *Exp Brain Res* 158: 265–277, 2004.

Roland J, Brunner P, Johnston J, Schalk G, Leuthardt EC. Passive real-time identification of speech and motor cortex during an awake craniotomy. *Epilepsy Behav* 18: 123–128, 2010.

Roopun AK, Simonotto JD, Pierce ML, Jenkins A, Nicholson C, Schofield IS, Whittaker RG, Kaiser M, Whittington MA, Traub RD, Cunningham MO. A nonsynaptic mechanism underlying interictal discharges in human epileptic neocortex. *Proc Natl Acad Sci USA* 107: 338–343, 2010.

Salazar AM, Jabbari B, Vance SC, Grafman J, Amin D, Dillon JD. Epilepsy after penetrating head injury. I. Clinical correlates: a report of the vietnam head injury study. *Neurology* 35: 1406–1414, 1985.

Salin P, Tseng GF, Hoffman S, Parada I, Prince DA. Axonal sprouting in layer V pyramidal neurons of chronically injured cerebral cortex. *J Neurosci* 15: 8234–8245, 1995.

Scharfman HE. The neurobiology of epilepsy. *Curr Neurol Neurosci Rep* 7: 1849–1857, 2008.

Schmidt-Heiber C, Jonas P, Bischofberger J. Action Potential initiation and propagation in hippocampal mossy fibre axons. *J Physiol* 586: 1849–1857, 2008.

Schmitz D, Schuchmann S, Fisahn A, Draguhn A, Buhl EH, Petrasch-Parwez E, Dermietzel R, Heinemann U, Traub RD. Axo-axonal coupling: A novel mechanism for ultrafast neuronal communication. *Neuron* 31: 831–840, 2001.

Schubert D, Kötter R, Luhmann HJ, Staiger JF. Morphology, electrophysiology and functional input connectivity of pyramidal neurons characterizes a genuine layer Va in the primary somatosensory cortex. *Cereb Cortex* 16: 223–236, 2006.

Scorcioni R, Polavaram S, Axcoli GA. L-measure: a web-accessible tool for the analysis, comparison and search of digital reconstructions of neuronal morphologies. *Nat Protoc* 3: 866–876, 2008.

Shepherd GMG, Svoboda K. Laminar and columnar organization of ascending excitatory projections to layer 2/3 pyramidal neurons in rat barrel cortex. *J Neurosci* 25: 5670–5679, 2005.

Shu Y, Duque A, Yu Y, Haider B, McCormick DA. Properties of action-potential initiation in neocortical pyramidal cells: Evidence from whole cell axon recordings. *J Neurophysiol* 97: 746–760, 2007a.

Shu Y, Hasenstaub A, Duque A, Yu Y, McCormick DA. Modulation of intracortical synaptic potentials by presynaptic somatic membrane potential. *Nature* 441: 761–765, 2006.

Shu Y, Yu Y, Yang J, McCormick DA. Selective control of cortical axonal spikes by a slowly inactivating K^+ current. *Proc Natl Acad Sci USA* 104: 11453–11458, 2007b.

Skoglund TS, Pascher R, Berthold CH. Heterogeneity in the columnar number of neurons in different neocortical areas in the rat. *Neurosci Lett* 208: 97–100, 1996.

Sloper JJ, Powell TP. A study of the axon initial segment and proximal axon of neurons in the primate motor and somatic sensory cortices. *Philos Trans R Soc Lond B Biol Sci* 285: 173–197, 1979.

Staba RJ, Bergmann PC, Barth DS. Dissociation of slow waves and fast oscillations above 200 Hz during GABA application in rat somatosensory cortex. *J Physiol* 561: 205–214, 2004a.

Staba RJ, Wilson CL, Bragin A, Jhung D, Fried I, Engel J Jr. High-frequency oscillations recorded in human medial temporal lobe during sleep. *Ann Neurol* 56: 108–115, 2004b.

Stacey WC, Lazarewicz MT, Litt B. Synaptic noise and physiological coupling generate high-frequency oscillations in a hippocampal computational model. *J Neurophysiol* 102: 2342–2357, 2009.

Staiger JF, Flagmeyer I, Schubert D, Zillis K, Kotter R, Luhmann H. Functional diversity of layer IV spiny neurons in rat somatosensory cortex: Quantitative morphology of electrophysiologically characterized and biocytin labeled cells. *Cereb Cortex* 14: 690–701, 2004.

Steriade M, Nuñez A, Amzica F. A novel slow (<1 Hz) oscillation of neocortical neurons in vivo: depolarizing and hyperpolarizing components. *J Neurosci* 13: 3252–3265, 1993.

Steriade M, Timofeev I, Grenier F. Natural waking and sleep states: a view from inside neocortical neurons. *J Neurophysiol* 85: 1969–1985, 2001.

Sutor B, Hagerty T. Involvement of gap junctions in the development of the neocortex. *Biochim Biophys Acta* 1719: 59–68, 2005.

Teskey GC, Valentine PA. Post-activation potentiation in the neocortex of awake freely moving rats. *Neurosci Biobehav Rev* 22: 195–207, 1998.

Timofeev I, Grenier F, Steriade M. Disfacilitation and active inhibition in the neocortex during the natural sleep-wake cycle: an intracellular study. *Proc Natl Acad Sci USA* 98: 1924–1929, 2001.

Traub R. Fast oscillations and epilepsy. *Epilepsy Curr* 3: 77–79, 2003.

Traub RD, Contreras D, Cunningham MO, Murray H, LeBeau FE, Roopun A, Bibbig A, Wilent WB, Higley MJ, Whittington MA. Single-column thalamocortical network model exhibiting gamma oscillations, sleep spindles, and epileptogenic bursts. *J Neurophysiol* 93: 2194–2232, 2005a.

Traub RD, Contreras D, Whittington MA. Combined experimental/simulation studies of cellular and network mechanisms of epileptogenesis in vitro and in vivo. *J Clin Neurophysiol* 22: 330–342, 2005b.

Traub RD, Cunningham MO, Gloveli T, LeBeau FE, Bibbig A, Buhl EH, Whittington MA. GABAenhanced collective behavior in neuronal axons underlies persistent gamma-frequency oscillations. *Proc Natl Acad Sci USA* 100: 11047–11052, 2003a.

Traub RD, Duncan R, Russell AJC, Baldeweg T, Tu Y, Cunningham MO, Whittington MA. Spatiotemporal patterns of electrocorticographic very fast oscillations (>80 Hz) consistent with a network model based on electrical coupling between principal neurons. *Epilepsia* 51: 1587–1597, 2010.

Traub RD, Pais I, Bibbig A, LeBeau FE, Buhl EH, Hormuzdi SG, Monyer H, Whittington MA. Contrasting roles of axonal (pyramidal cell) and dendritic (interneuron) electrical coupling in the generation of neuronal network oscillations. *Proc Natl Acad Sci USA* 100: 1370–1374, 2003b.

Traub RD, Schmitz D, Jefferys JG, Draguhn A. High-frequency population oscillations are predicted to occur in hippocampal pyramidal neuronal networks interconnected by axoaxonal gap junctions. *Neuroscience* 92: 407–426, 1999.

Traub RD, Whittington MA, Buhl EH, LeBeau FE, Bibbig A, Boyd S, Cross H, Baldeweg T. A possible role for gap junctions in generation of very fast EEG oscillations preceding the onset of, and perhaps initiating, seizures. *Epilepsia* 42: 153–170, 2001.

Tsumoto T. Long-term potentiation and depression in the cerebral neocortex. *Jpn J Physiol* 40: 573–593, 1990.

Tuckwell HC. *Introduction to Theoretical Neurobiology: Volume 1, Linear Cable Theory and Dendritic Structure*. Cambridge, UK: Cambridge University Press, 1988.

Urrestarazu E, Chander R, Dubeau F, Gotman J. Interictal high-frequency oscillations (100–500 Hz) in the intracerebral EEG of epileptic patients. *Brain* 130: 2354–2366, 2007.

Wang W, Degenhart AD, Collinger JL, Vinjamuri R, Sudre GP, Adelson PD, Holder DL, Leuthardt EC, Moran DW, Boninger ML, Schwartz AB, Crammond DJ, Tyler-Kabara EC, Weber DJ. Human motor cortical activity recorded with micro-ECoG electrodes, during individual finger movements. *Conf Proc IEEE Eng Med Biol Soc* 2009: 586–589, 2009a.

Wang Y, Barakat A, Zhou H. Electrotonic coupling between pyramidal neurons in the neocortex. *PLos One* 5: e10253, 2010.

Wang Y, Gupta A, Toledo-Rodriguez M, Wu CZ, Markram H. Anatomical, physiological, molecular and circuit properties of nest basket cells in the developing somatosensory cortex. *Cereb Cortex* 12: 395–410, 2002.

Wang Y, Zhang G, Zhou H, Barakat A, Querfurth H. Opposite effects of low and high doses of A β42 on electrical network and neuronal excitability in the rat prefrontal cortex. *PLos One* 4: e8366, 2009b.

Waxman SG, Kocsis JD, Stys PK. *The Axon: Structure, Function, Pathophysiology*. Oxford, UK: Oxford University Press, 1995.

Worrell GA, Gardner AB, Stead SM, Hu S, Goerss S, Cascino GJ, Meyer FB, Marsh R, Litt B. High frequency oscillations in human temporal lobe: Simultaneous microwire and clinical macroelectrode recordings. *Brain* 131: 928–937, 2008.

Worrell GA, Parish L, Cranstoun SD, Jonas R, Baltuch G, Litt B. High-frequency oscillations and seizure generation in neocortical epilepsy. *Brain* 127: 1496–1506, 2004.

Ylinen A, Bragin A, Nádasdy Z, Jandó G, Szabó I, Sik A, Buzsáki G. Sharp wave-associated high-frequency oscillation (200 Hz) in the intact hippocampus: network and intracellular mechanisms. *J Neurosci* 15: 30–46, 1995.